UNIVERSITÀ POLITECNICA DELLE MARCHE

FACOLTÀ DI INGEGNERIA

Corso di Laurea Magistrale in

BIOMEDICAL ENGINEERING

Evaluation of a model to detect vital signs of a subject trapped in hard-to-reach environment using a laser doppler vibrometry technique

Supervisor:

Prof. Lorenzo Scalise

Thesis Written By:

Calvin Abonga

Academic Year 2021/2022

ACKNOWLEDGEMENT

First and foremost, I want to thank God the almighty for seeing me through this project. Secondly, I want to express my deepest appreciation to my supervisor Professor Lorenzo Scalise for his constant motivation, inspiration and, guidance throughout the journey of this study. In a special way, I want to pour out my heartfelt gratitude and appreciation to my co-supervisor Engineer Luca Antognoli for his time, guidance, and tireless assistance while carrying out the experiments and analyzing the data for this study. This study would not have been possible without my classmates and friends who voluntarily accepted to take part in it and others who helped in data analysis, thank you very much and may God largely reward you all. I also want to extend my gratitude to the UNIVPM fraternity for availing me the opportunity to expand my skill sets through Flor scholarship and the DIISM for accommodating me in their laser laboratories throughout this study. Lastly but not the last, I want to thank my parents and family members who constantly supported me with words of encourage and prayers which saw me through this journey.

ABSTRACT

Vital signs detection and monitoring is very key for monitoring the state of life for a patient in a clinical setting or subject trapped in a hard-to-reach environment like war zone, radiation leaked areas etc. In the clinical setting, the contact method is widely used whereas in the hard-to-reach environment, the most feasible method is contactless. In this study, cardiorespiratory signal was acquired contactlessly using the Laser doppler vibrometer (LDV). The experiment recruited 17 subjects and 213 data sets of 60 second long were obtained. The LDV signals were preprocessed by filtering out noise at 40Hz, heart rate between (1 to 5 Hz), and Respiratory rate at (0.1 to 0.5Hz). Features extracted from the signal included, power spectral density (PSD), root mean square (RMS), peak to peak intervals. Using the PSD, the behavior of the signal with various variables of distances, angles, anatomical positions, skin color and cloth tightness were analyzed as shown in Figure 11-16. Data was then divided into two set. One set was for data obtained horizontally from the chest position at a standard distance of 0.5m and angle of 0 degrees. The other set had data collected from all the protocol variables used in this study. Data from random environmental objects and a resuscitation baby mannequin were as well acquired to simulate a hard-to-reach environment and a dead person. The two data sets were used to create two databases in .cvs format. 70% of both databases was used in training the model and 30% for model validation using a decision tree algorithm with 8 nodes and 42 random. Model 1 produced a classification accuracy of 89.0% and model 2 presented an accuracy of 92.0% when classifying data from the random objects and baby mannequin with data from the human subjects. The second model had the best performance when compared to the first model due to the presence of a large data set.

Table of Contents

Contents

List of Figures

List of Tables

Nomenclature

This is a description of several acronyms used within the texts
LDV = Laser Doppler Vibrometer
MRI = Magnetic Resonance Imaging
ECG = Electrocardiography
PPG = Photoplethysmography
LED = Light Emitting Diodes
iPPG = Imaging photoplethysmography
UWB = Ultra-Wide Band
AD Instrument = Analog to Digital Instrument
MATLAB = Matrix Laboratory
DIISM = Department of Industrial Engineering and Mathematical Science
UNIVPM = Universita Poltechnica Delle Marche
RMS = Root Mean Square
PSD = Power Spectral Density

CHAPTER 1

1. INTRODUCTION

Detection and continuous monitoring of human physiological vital signs, like heartrate and breath rate, plays a very crucial role in predicting the state of a human being health and wellbeing. Heart rate is the number of beats produced by the heart under one minute whereas breath rate is the frequency of respiration cycle accomplished under one minute by an individual. The normal heart rate and breath rate of an adult is 60-100 beats per minute and 12-20 breaths per minute [2,3,4]. These vital signs are both detected and monitored either with contact or non-contact methods [2]. It is however quite challenging to detect and monitor these signals in hard-to-reach environments like war zones, radiation leaked sites, MRI rooms, infectious sites etc. using the contact methods because of gun shots fear, biochemical hazards exposure, MRI hazards and biological hazards exposure respectively. According to [1], about 100,000 soldiers are reported dead at battle fronts annually around the globe. These numbers could be reduced exploiting the potential contactless methods offer especially Laser doppler vibrometry technique.

1.1. Contact based method of cardiorespiratory vital sign monitoring and detection

This method of cardio-pulmonary vital signs monitoring involves the attachment of sensors or contact electrodes directly on the subject's body to acquire the heart rate and breath rate signals. These methods have their short comings when they are to be applied no subjects in hard-to-reach environments as it will be discussed shortly. The following contact-based methods are discussed; electrocardiography, photoplethysmography, ballistocardiography, and Capnography.

1.1.1. Electrocardiography.

Electrocardiography is the process of generating heart beats from the electrical activity of the heart while placing electrodes on defined anatomical landmarks of the body [5]. An Electrocardiograph (ECG) is the signal generated and it is usually meant to monitor heart rate (Figure 1c), however, breathing rate can as well be extracted from it [16, 17], using the sinus arrythmia process [8]. The 12 lead ECG which is the gold standard for heart rate monitoring (Figure 1a) and the portable ambulatory ECG (Figure 1b) are the most common systems of ECGs.

Just like any type of ECG, these two common types require the placement of electrodes on the subject's body and are then connected to a processing unit either wirelessly or with cables which are often done in clinical settings. The process of electrode placements requires an access to a subject by the third party and this is almost impossible due to the dangers it poses or time consuming when one is trapped in a hard-to-reach environment. In other cases, like for burns patients, elderly, and neonates whose skins are very delicate, the electrodes might cause ulcerations, discomfort, strangulation, and irritations among others [9].

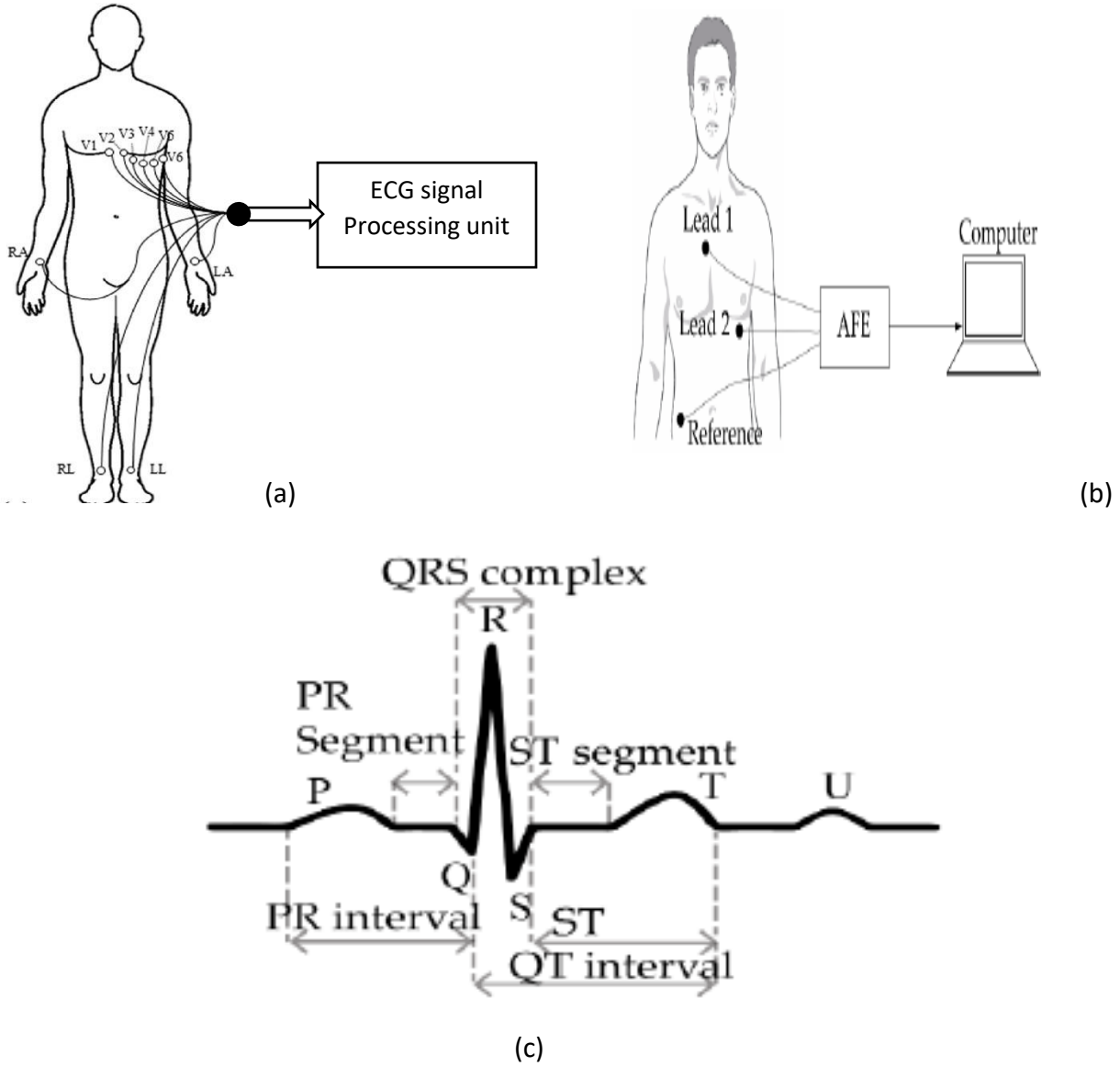

Figure 1: (a) 12 lead ECG lead system (Image obtained from [2]). (b) Ambulatory ECG system (Image obtained from [2]). (c) ECG signal (Image obtained from [2])

1.1.2. Photoplethysmography

Photoplethysmography (PPG) is an optical technique that measures and detects blood volume changes in tissues' microvascular bed due to each heartbeat (Figure 2). Photoplethysmograph is the signal obtained from photoplethysmography [10]. For this method, usually one or more Light emitting diodes (LED) sensors are directly placed on the anatomical position of interest like the hand wrist, fingers, ear lobes and toes. The wavelengths of the light emitted by the diodes are between 500 nm and 600nm which corresponds to yellow and green optical region [11]. And most photoplethysmography make use of the green light to acquire heart rate signals. The red and infra-red regions in most photoplethysmography device are used for monitoring blood oxygen saturation [12].

The photodetector which is meant to receive and detect the vital signs is positioned depending on the acquisition mode. If the acquisition is in the reflectance mode, the photodetector is placed on the same side with the light emitting diode and for the transmission mode, the photodetector is placed on the opposite side to the light emitting diode [13]. In addition, the technique can as well be used to estimate respiratory rate because breathing causes changes in the amplitude and frequency of the signal [13]. Despite the contribution of PPG in cardiorespiratory vital signs monitoring, its limitations in hard-to-reach environment are quite similar to those presented by the ECG methods, since all require the placement of sensors directly on the subject's skin.

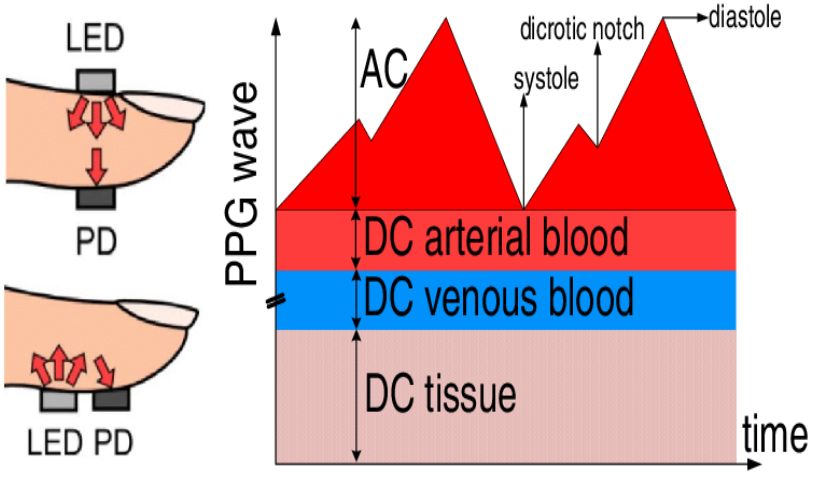

Figure 2: PPG measurement set ups and the DC and AC component of the signal generated (Image was obtained from [32]).

1.1.3. Ballistocardiography

Ballistocardiography is a method that relies on the movements of the chest or body due to the contraction of the diaphragm and the heart allowing the flow of air into the lungs and blood to the whole body respectively. These displacements account for up to 7.37cm chest expansion circumferentially [14]. Most sensors used to measure these displacements are based on strain sensing, impedance pneumography, and movement sensing using gyroscopes, accelerometers, and magnetometers. This technology portrays limitations of strapping the sensors on the subject's body prior to monitoring and detection of cardiopulmonary vital signs in hard-to-reach environments. The fabrics holding the sensors could as well cause skin irritations and ulcerations among the elderlies and neonates as well.

1.1.4. Capnography

Capnography is a system made up of carbon dioxide sensors, a gas sampling tube, and a signal processing unit (Figure 3) used to detect the amount of carbon dioxide that we inhale and exhale at each breath [16]. Most of the systems use infra-red and fiber optic sensors. The setup of these systems can be side stream, in which the sensors and the main processing unit are placed away from the subject and in contrast, mainstream in which the sensors are between the processing unit and endotracheal tube [15]. This method is unique in the sense that motion artifacts doesn't affect it however, the chemicals in the sensors could react to other gases, its sensitivity varies basing on temperature, and humidity of the environment as well [17]. In the hard-to-reach environment, this method is impractical because it requires setting up the test on the subject by the third party.

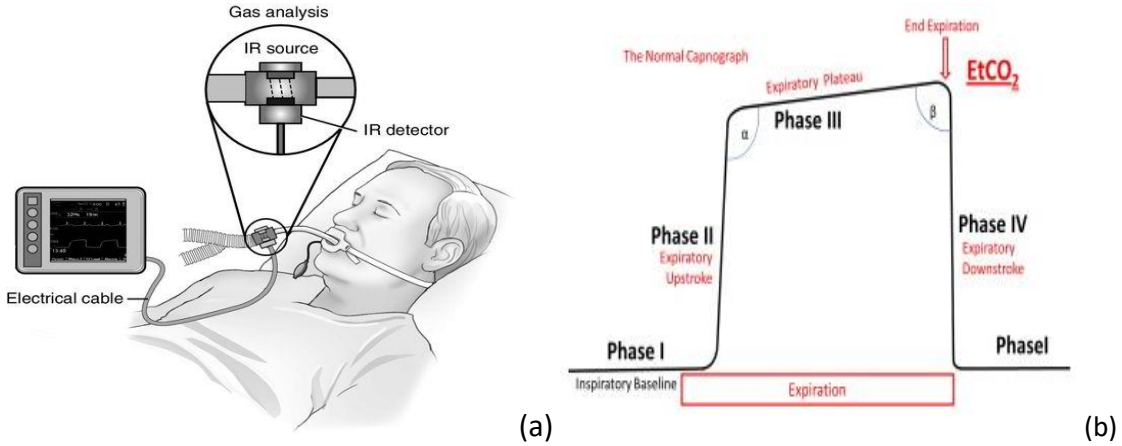

(a) (b)

Figure 3: (a) Capnography device setup (Image obtained from https://aneskey.com/capnography-monitoring/). (b) Signal of capnography (Image obtained from [34])

1.2. Contactless based method of cardiorespiratory vital sign monitoring and detection

This method of cardiorespiratory vital signs monitoring depends on the subtle movements and other variability on specific anatomical landmarks across the body because of the mechanical actions of the lungs and heart. To acquire these signals, techniques utilizing the doppler effect, thermal imaging and camera imaging are being exploited.

1.2.1. Thermal Imaging

Thermal imaging relies on modulating radiations from different anatomical positions of the body to detect cardiorespiratory signals [2]. The best operating spectrum of this method is infrared and the major four bands utilized are: near infrared (0.75 to 3 μm), middle infrared (3-6μm), far infrared (6-15 μm) and, extreme infrared (15-100 μm) [18, 19]. To predict cardiac activity, the thermal imaging technique detects the slight heat variability caused by the pulsating blood flowing in the major superficial arteries in certain anatomical sites. And sensing the respiratory signal requires detecting small temperature variability around the nostrils using the thermal camera. This method of non-contact measurement is very advantageous in acquiring signals from some anatomical locations and works well under low illumination. The challenges posed by thermal imaging are mainly related to temperature variability and this becomes very impractical in the hard-to-reach environments. In addition, the signals from the subjects are also affected by the motion artifacts and the camera can only detect signal at short distance.

1.2.2. Camera imaging

The camera imaging technique is divided into color-based method and motion-based method. The color-based method of camera imaging works using the principle of photoplethysmography of light transmittance and reflectance due to due blood volume [20]. This technique is called imaging photoplethysmography (iPPG) and can be used to detect both cardiac and respiratory activities (Figure 4). A dedicated video camera is used as a photodetector which could be having the light emitting source embedded with it in case of a reflectance principle or an independent light source when using the transmittance principle. The color-based method is associated with various advantages such as reliability of results when subject is still or in motion, possibility of performing multiple signal acquisitions from various subjects in a short time. However, the

signals are obtained using this method is affected by skin color tone, and image focus. Signals can only be acquired at short distances and depth.

In motion-based method of imaging, a video camera is used to capture small amplitude motions that are caused by the mechanical actions of the heart and lungs [21]. The images and videos are then processed to extract data that are used to predict respiratory rate and heart rate. The two most important components in this method are the type of camera and a signal processing algorithm or method used. This method is not affected by skin color tone or physical barrier like cloth during monitoring. However, the problems faced by this method includes motion artifacts and short-range operation distances.

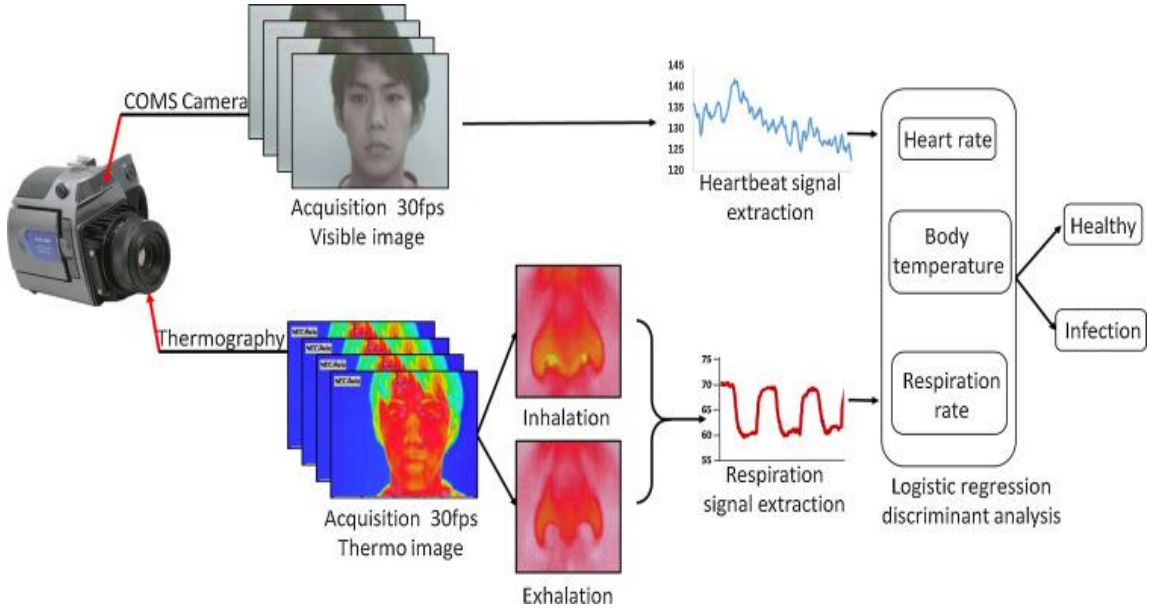

Figure 4: Illustrations of cardiorespiratory signal acquisitions using COMS camera (Image obtained from [34]).

1.2.3. Electromagnetic radar-based method

Electromagnetic radar-based method of human physiological vital signs detection and monitoring is divided into; continuous wave, frequency modulated (FM) and ultra-wide band (UWB) technique [2]. The continuous wave radar systems are the simplest and most common types of electromagnetic radar-based method that has a transceiver with both a transmitting and receiving antenna. The transmitter antenna sends a continuous wave of signal to the human anatomical position of interest and the reflected signal is captured by the receiver. Through demodulation and processing signal, heart rates and respiratory rates are extracted from the

received signal [2]. The equations illustrating the time domain transmitted signal denoted by T(t), received signal denoted by R(t), and the instantaneous displacements denoted by x(t) are illustrated below [2].

$$T(t) = A_t Cos(\omega t + \varphi(t)), \quad (1)$$

$$R(t) = A_r Cos[\omega t - \frac{4\pi}{\lambda}(d_0 + x(t)) + \varphi(t - \frac{2d0}{c})], \quad (2)$$

$$x(t) = A_b Cos(\omega_b t + \varphi_b) + A_h Cos(\omega_h t + \varphi_h), \quad (3)$$

where At and Ar, ω, λ, c, d0, Ab, Ah, ϕ_b, ϕ_h are the amplitudes of transmitted and received signals, angular frequency of transmitted signal, the carrier wavelength, the speed of light, the constant distance between the antennas and the subject, amplitudes, and phase shifts of the chest displacement due to breathing and heartbeat respectively [2].

The frequency modulated radar (FM) systems are classified into the frequency modulated continuous wave (FMCW) radars and the stepped frequency continuous wave (SFCW) radars [2]. For the FMCW radar systems, the frequency of the signal output with respect to time is linear and in SFCW radars, the output signal compromises of N frames that are linearly transmitted to the surface of interest with an interval of Δf between each frame. The transceiver architecture of all frequency modulated radar systems is like that of continuous wave radar systems and as well their operations. To decrease the high computational workload of these systems, the received signals are directly converted with a replica of the transmitted signal [22]. Beat signal is a demodulated signal containing both the range and micro-doppler information. The data is usually put in a matrix form containing both the slow time and fast time data. The data containing the vital signs information of interest is the fast time data which indicates the number of samples per ramps.

The pulse-based sensing modules like Impulse radio ultra-wideband radar (IR-UWB) relies on sending a short pulse of modulated or unmodulated pulse to the subject by the radar's transmitter. The signals or pulse reflected by the subject is captured by the receiver antenna and processed into useful cardio-respiratory signals [23]. All the discussed methods of electromagnetic radar-based methods are advantageous when being used in hard-to-reach environments because of the contactless acquisition and processing of the cardiorespiratory signals in addition to their ability to consume low power and ability to penetrate non-conductive

materials. Short distance applications, signal to noise ratio is low, and motion artifacts are among the main limitations of radar-based methods

1.2.4. Laser radar-based methods

Just like electromagnetic radar-based technique, the laser doppler vibrometry/ velocimetry operates using the principle of doppler shift to obtain information generated from a vibratory surface and interferometry of signals [24]. The laser doppler vibrometry (LDV), is an optical technique known to have a very high spatial resolution and temporal coherence, allowing displacement measurements of up to 8 nm [25]. And a laser doppler vibrometer is an optical interferometer device that splits a laser beam into a reference beam and a measurement beam [26]. During signal acquisition, a measurement beam with a frequency fo is directed onto the target surface. The reference beam is recombined with a reflected beam having a frequency shift of fd which is proportional to the target surface velocity in the detector [27]. A Bragg cell is very useful in distinguishing if the detected vibration is away or towards the laser by shifting the frequency of reference laser by fb.

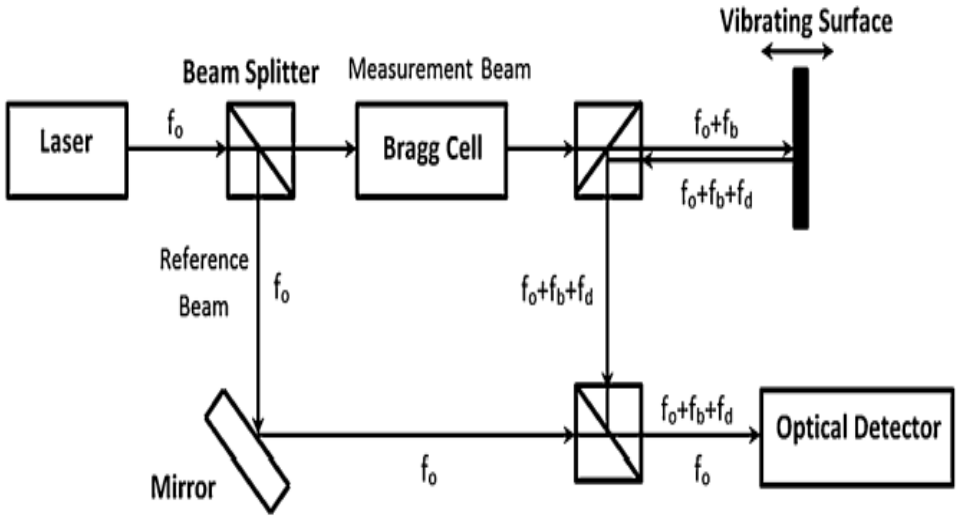

Figure 5: Image illustrating the working principle of a laser doppler vibrometer. Imaged was obtained from [27]

The LDV method is very advantageous in hard-to-reach environments because they can operate at large distances of more than 10meters [28], high resolutions, and low power density requirement [31]. Despite their advantages, LDV do suffer demerits of high cost and motion artifacts.

1.3. Aims of the study

Many literatures on laser doppler vibrometry have been published extracting cardiorespiratory vital signs. One such study was by Scalise and Morbiducci [28], using LDV to detect cardiac activity with the subject at 1.5m while pointing the laser beam to the neck on the carotid artery. Other studies investigated respiratory activity by measuring the chest wall displacements in adults [29] and infants [30]. Marchionni et al. [31], as well extracted cardiorespiratory signals of infants while in incubators at a distance between 1-2m. These studies illustrated the potential that LDV technology holds especially in monitoring and detecting cardiorespiratory signals of subjects trapped in hard-to-reach environments and formed the basis of this study.

The main purpose of this study was to develop an model that can be used to detect the state of life and the vital signs of a subject trapped in a hard-to-reach environment using a laser doppler vibrometry technique. To achieve this goal, other sub objectives were set for evaluation; (1) To determine the effect of skin color variability on the signal strength, (2) To determine the effect of cloth tightness on the signal strength, (3) To determine the optimal distance for LDV operation and their effects on signal strength, (4) To determine the effect of angle of acceptance's variability on the strength of LDV signal, (5) To evaluate the potential of using other anatomical sites for signal acquisition. Data collected from the LDV device will be evaluated against finger pulse reader and a standard breathing protocol of 4s per breath for heart rate and respiratory rate signal respectively.

CHAPTER 2

2. MATERIALS AND METHODS

2.1. Materials

The materials used in this study included a laser doppler vibrometer (LDV), AD Instrument 's hardware and software (Labchart) for digital to analog conversion and sampling, Personal computer (PC), Finger pulse reader, a resuscitation baby mannequin, MATLAB and python software for data analysis, breathing application, tripod stand for holding the LDV, chair and a stretchable bed for allowing the subject to relax during testing.

2.2. Study population

A total of 17 young healthy subjects were recruited for the study and for each subject, more than 9 data points with a duration of 60 seconds for each were collected while changing the protocols to meet the set objectives. 12 of the subjects were young male and 5 were young female, with the mean age of 24 and body mass index in the range of 18.2 to 24.9. The overall number of data collected from all the subjects were 213. For inclusion into the study, the subject must be an adult who is healthy and is of sound mind. Any subject who was unhealthy on the day of data collection was excluded from the study. In addition, 21 data points were collected from a resuscitation baby mannequin and 30 data points were collected from random objects to simulate a dead person and the surroundings of hard-to-reach environments. This study was performed in the department of Industrial Engineering and Mathematical Sciences (DIISM) at Universita Politecnica Delle Marche.

2.3. Experimental setup

The experiment was performed on 17 healthy subjects, with each acquisition lasting one minute. 13 subjects were told to relax and breath normally while 4 subjects were asked to breath at a regular interval of 4 seconds during signal acquisition. Each of the subjects followed the defined procedures afterwards

- A subject was asked either to lie still while looking up with eyes closed on a bed or sit upright on a chair and the LDV's laser beam is positioned directly over them (Figure 27 and 28 in appendix).
- six anatomical sites were selected for the study i.e., head, chest, stomach, arm, leg, and foot with no specificity within the sites (Figure 29 in appendix).

- The head, arm, stomach, leg, and foot anatomical sites are investigated at a constant distance of 0.5m, angle of 0^o, directly on the skin as illustrated in Table 1.
- Whereas the chest position was investigated while varying distances, angles, skin color using the Fitzpatrick scale (Table 2) and fabric tightness on the skin.
- The Cardiorespiratory signal obtained was then validated using a pulse finger reader and a standard breath holding protocol of 4 seconds.

Table 1: The various anatomical sites and positions investigated for physiological vital signs using the LDV technology while varying the distances, angles, cloth sizes and skin tone for the chest region on a Human subject

Anatomical body sites	Distance (meters)	Angle (Degrees)	Cloth Tightness (L=Loose, T=tight)	Skin Color scale (I, II, III, IV, V, VI)
HEAD	0.5	0	N/A	N/A
CHEST	0.5 1 2 3 5	0 10 20 30 40 45 60 70 80	L T	
STOMACH	0.5		N/A	N/A
ARM	0.5	0	N/A	N/A
LEG	0.5	0	N/A	N/A
FOOT	0.5	0	N/A	N/A

Table 2: The FITZPATRICK SCALE used in the classification of skin color/tone

FITZPATRICK TYPE	DESCRIPTION
I	Very light or white. “celtic” type
II	Light or light-skinned European
III	Light intermediate, or dark-skinned European
IV	Dark intermediate or “Olive skin”
V	Dark or "brown" type
VI	Very dark or "black" type

2.4. Signal acquisition

To collect data, the experiments were set up as shown in Figure 27 and 28 in the appendix below. When the subject is well relaxed in an upright seated position or lying position, the laser beam generated by the LDV device is then pointed to the anatomical site under study. The laser Doppler vibrometer (Polytec, PDV100, GmbH, Germany) allows the measurement of instantaneous velocity (amplitude and direction) of the surface where the laser spot is focused. The laser sensor works with a He–Ne laser source (632.8 nm). As for safety precautions, the LDVi is a Class II B device, so that no special safety measures are required (laser power is less than 1 mW). The reflected beam from the

site is detected by the LDV device and sampled at a frequency of 1000Hz using an analog to digital instrument Acquisition board. The data generated by the AD Instrument is recorded and visualized by Labchart software. From this software tool, the data is then exported for storage and analysis on the MATLAB software on a computer. The same procedure of data collection is followed for the pulse reader since it is directly connected to the AD Instrument using another channel. The specifications of the LDV that is required during experiment setup is shown below.

2.5. Data Processing and Analysis

The acquired data was first preprocessed on MATLAB R2021b version toolbox. This involved wavelet decomposition using 7 decibels (db 7) and 12 levels of decomposition of the signal to understand its frequency and power distribution. It was followed with filtering of noise, heart rate, respiratory rate at a cut off frequency of 40hertz, 1-4hert, and 0.1-0.5Hertz respectively using low and high pass Butterworth filter of order 4. The same protocol was followed for the baby mannequin data. The clean data were then subjected to statistical analysis using MATLAB to visualize the effects of the various variables like angles, distances, skin color, cloth tightness and anatomical positions on the signal strength and power. Features like peaks and locs, peak to peak intervals, displacements due to the heart rate and respiration, root mean square values and power spectral density were obtained from the data as well. To obtain the respiratory and heart rates from the signal, the peak-to-peak interval feature was multiplied by 60 seconds as shown in the formulas below. The numbers of beats and respiratory cycles from each data point were compared against the results from finger pulse reader and the standard breathing protocol of 4s to validate this protocol.

$$Heat\ rate\ (HR) = \left(\frac{1}{peak{-}peak\ interval\ in\ seconds}\right) * 60 \quad (4)$$

$$Respratory\ Rate\ (RR) = \left(\frac{1}{peak{-}peak\ interval\ in\ seconds}\right) * 60 \quad (5)$$

2.6. Model development

All the signals acquired from both the LDV, baby mannequin and environmental objects were subjected to database creation. Two databases were created, with the first one using 20 signals acquired horizontally from the chest of a subject, 15 from environmental objects, and 5 from the baby mannequin. The second database had all the 213 signals acquired from all the different

protocols of the study, 30 from environmental objects and 21 from the baby mannequin. For the first database, a portion of 50 samples from each signal was acquired randomly 100 times and the second database had a portion of 50 samples from each signal sampled randomly 49 times. The samples in text files format were then converted to the cvs format for machine learning.

The decision tree algorithm with 8 nodes and 42 random states as a machine learning platform was then used to create a model and validate it. For model creation, python version3.10 was used utilizing the scikit learn toolbox. Two models were developed. Model 1 using the first database and model 2 using the second database of data. Each of the model utilized 70% of its database for training and 30% of its remaining database to validate the model created. The models were later tested on all acquired data sets from the 17 subjects and their accuracies with respect to the various variables affecting the LDV signals were plotted and analyzed.

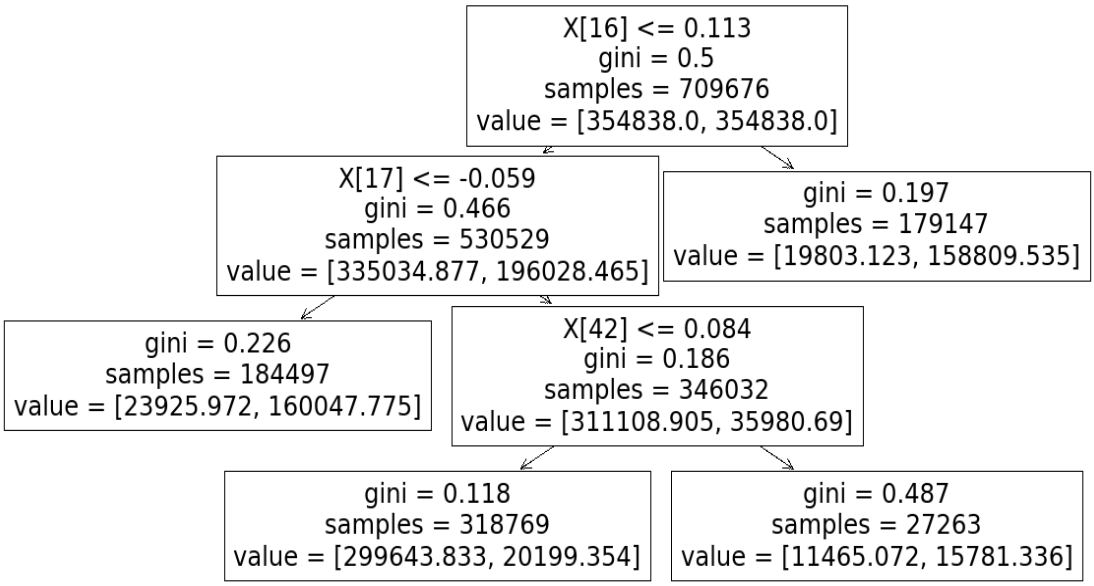

CHAPTER 3

3. RESULTS

3.1. Signal Acquisition and representation

Wavelet decomposition

Levels of wavelet Decomposition	D1	D2	D3	D4	D5	D6	D7	D8	D9	D10	D11	D12
Frequency Range (Hz)	250 - 500	124 - 252	61.9 - 126	31 - 63.1	15.5 - 31.5	7.74 - 15.8	3.87 - 7.89	1.93 - 3.94	0.967 - 1.97	0.484 - 0.986	0.242 - 0.493	0.122 - 0.246
Relative Energy (%)	0.73	0.55	0.52	0.53	0.75	1.63	2.65	7.75	35.29	36.00	11.32	1.98

Figure 6: Wavelet decomposition levels. Red color is a representation of frequency range for respiratory signal and green is for heart rate

Raw LDV and Pulse signal

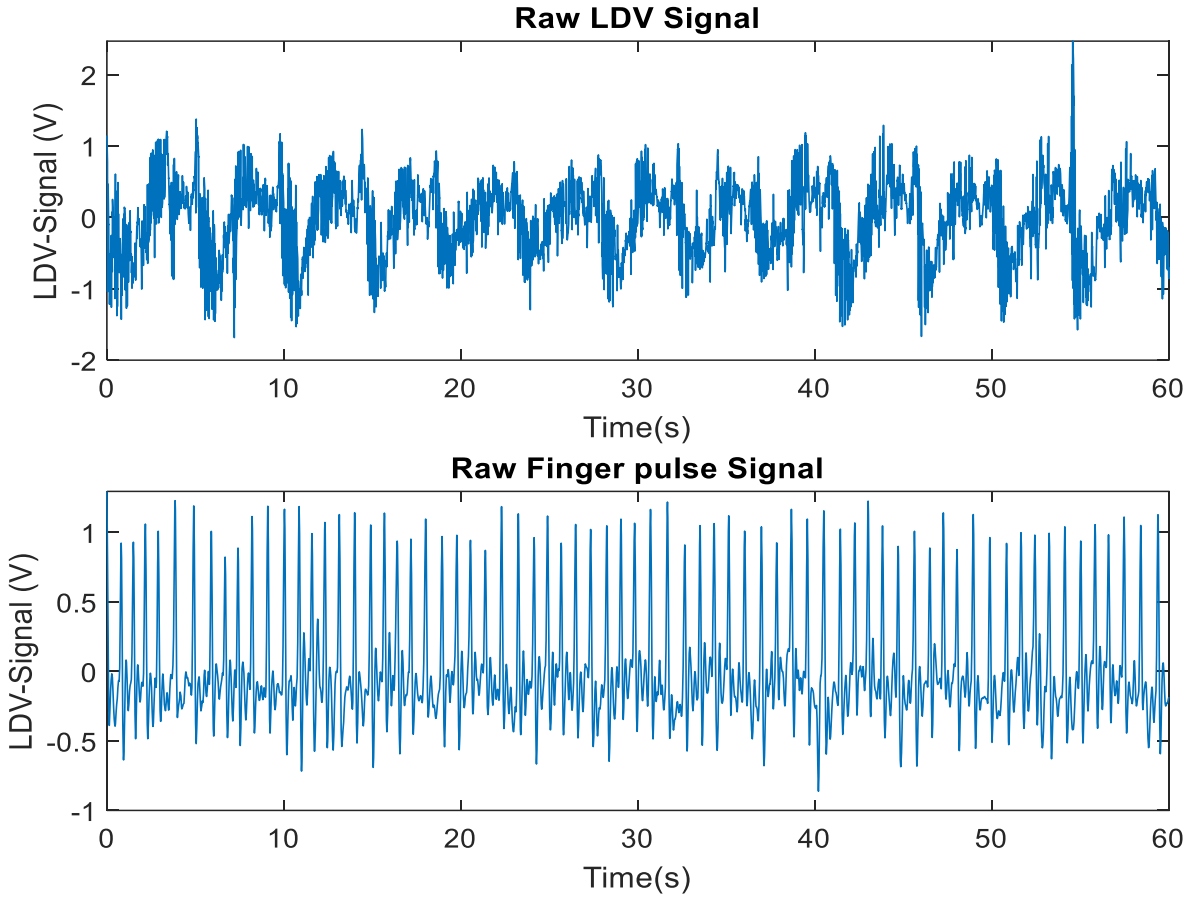

Figure 7: Representation of Raw LDV and pulse reader signal acquired from the chest of 1 subject

Filtered Heart rate and respiratory rate from different anatomical positions

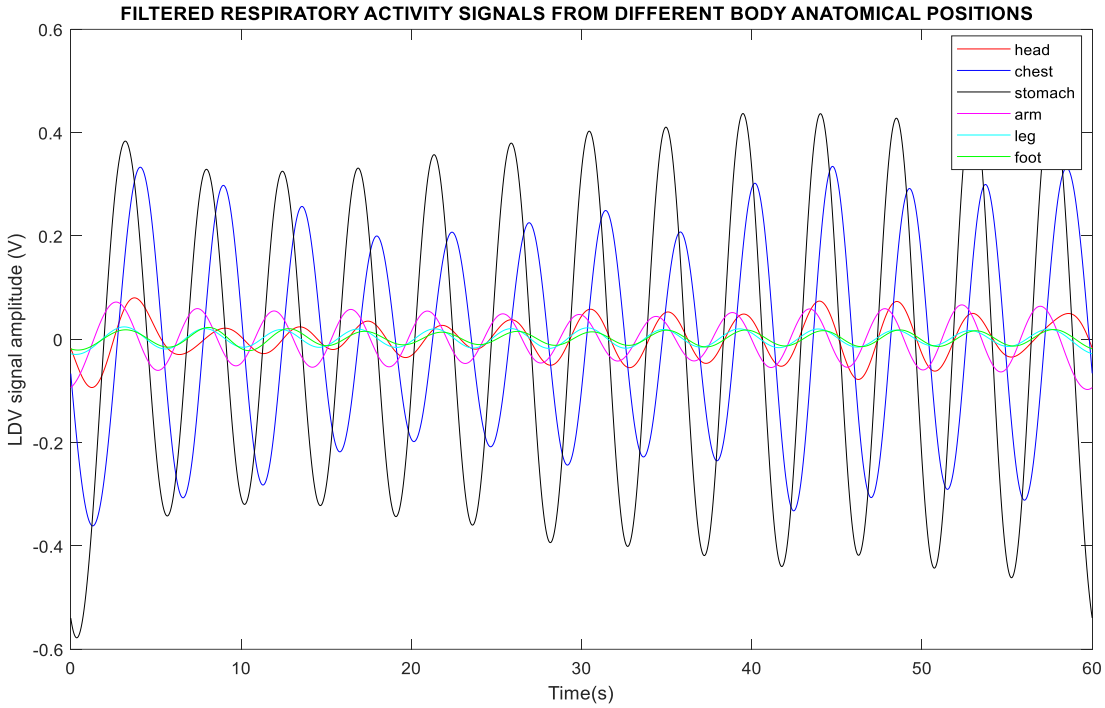

Figure 8: Filtered Respiratory activity across the different anatomical positions

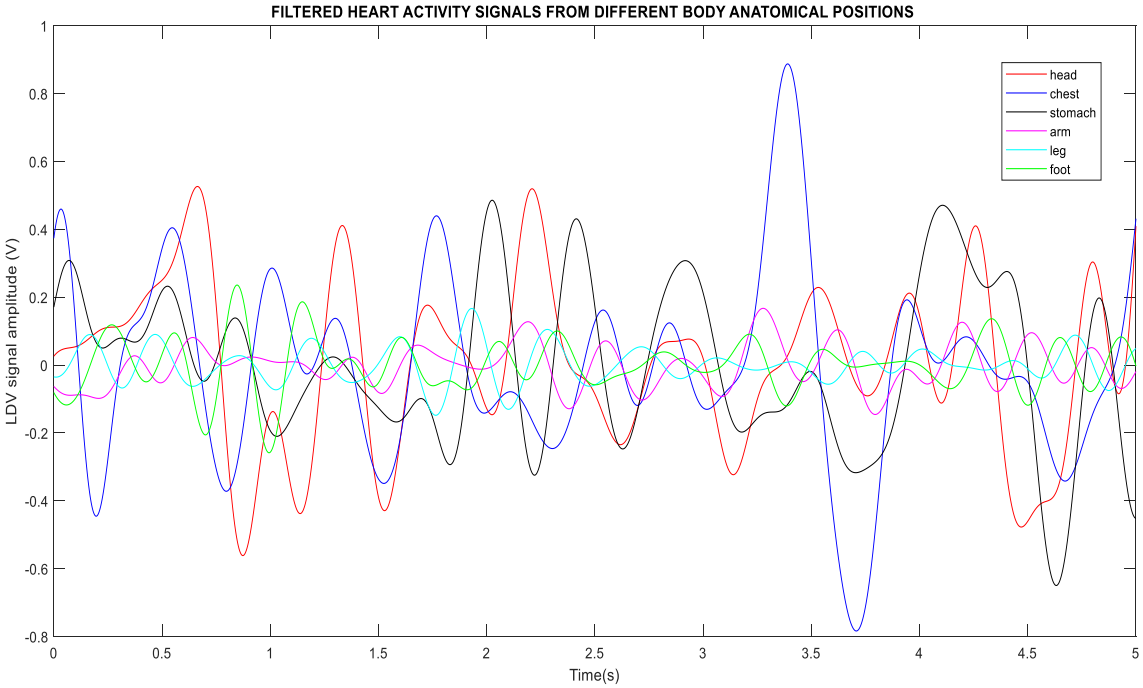

Figure 9: Filtered Heart activity across the different anatomical positions

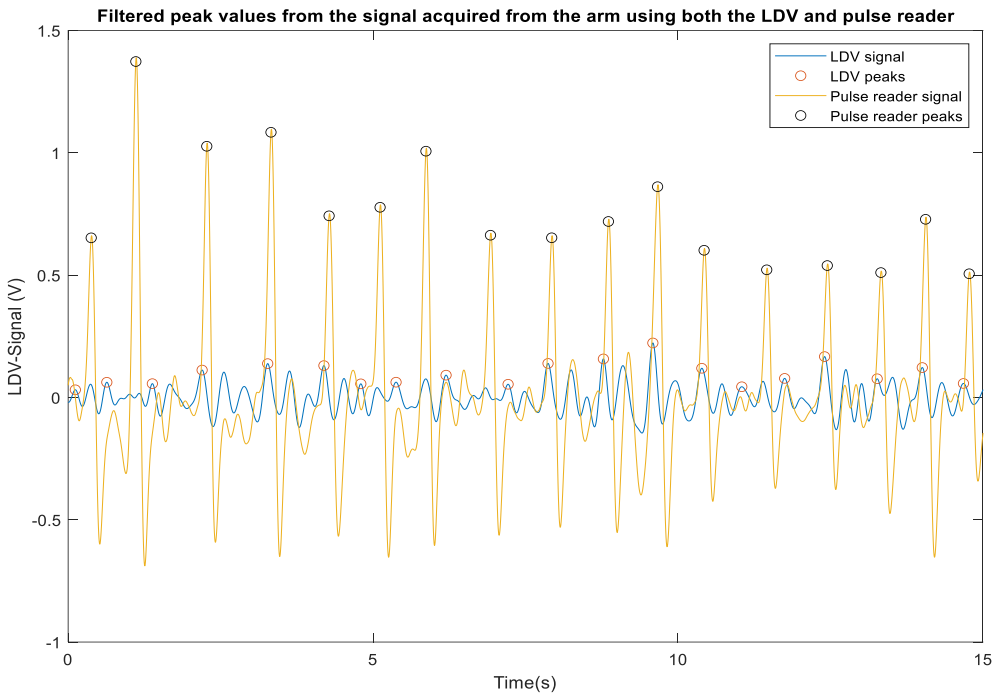

Figure 10: A comparison of the peak numbers and their positions extracted from both the LDV and finger pulse sensor reader

3.2. Variability of the LDV signal power spectral density with the various distances from the LDV device

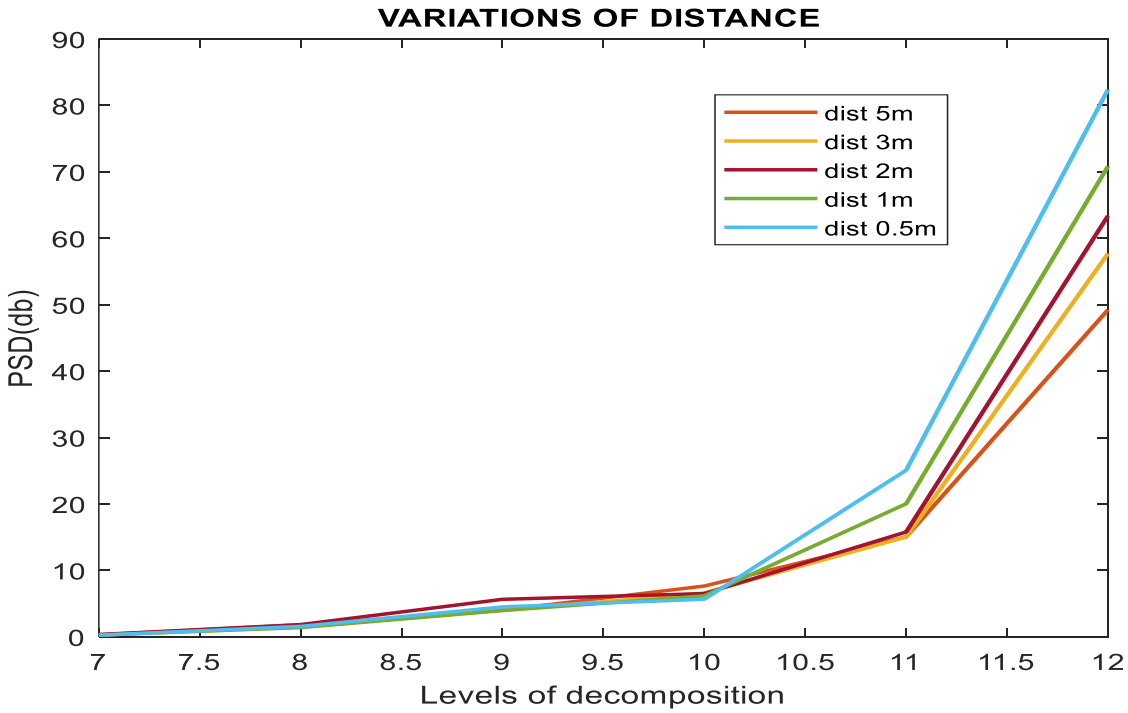

Figure 11: Variations of different distances with LDV'S power spectral density

Variability of acceptance angles to the LDV device

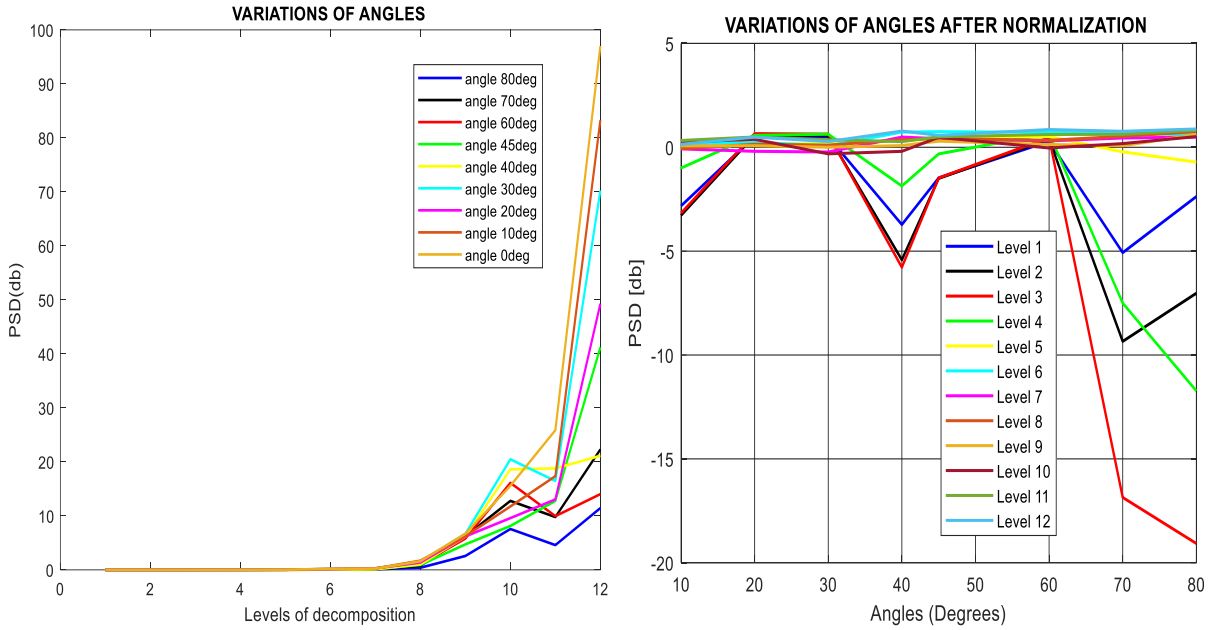

Figure 12:Variability of LDV's power spectral density distribution with angles.

Variability of different anatomical positions with LDV's power spectral density

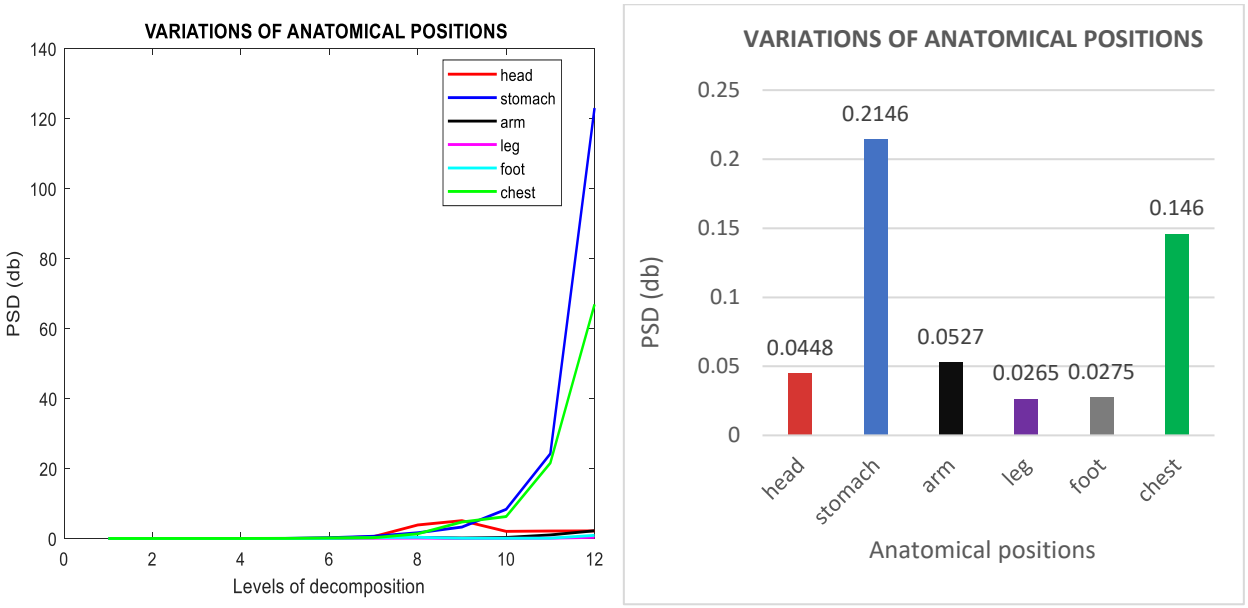

Figure 13: Variability of LDV's power spectral density distribution with different anatomical positions.

Variability of LDV's power spectral density with cloth tightness

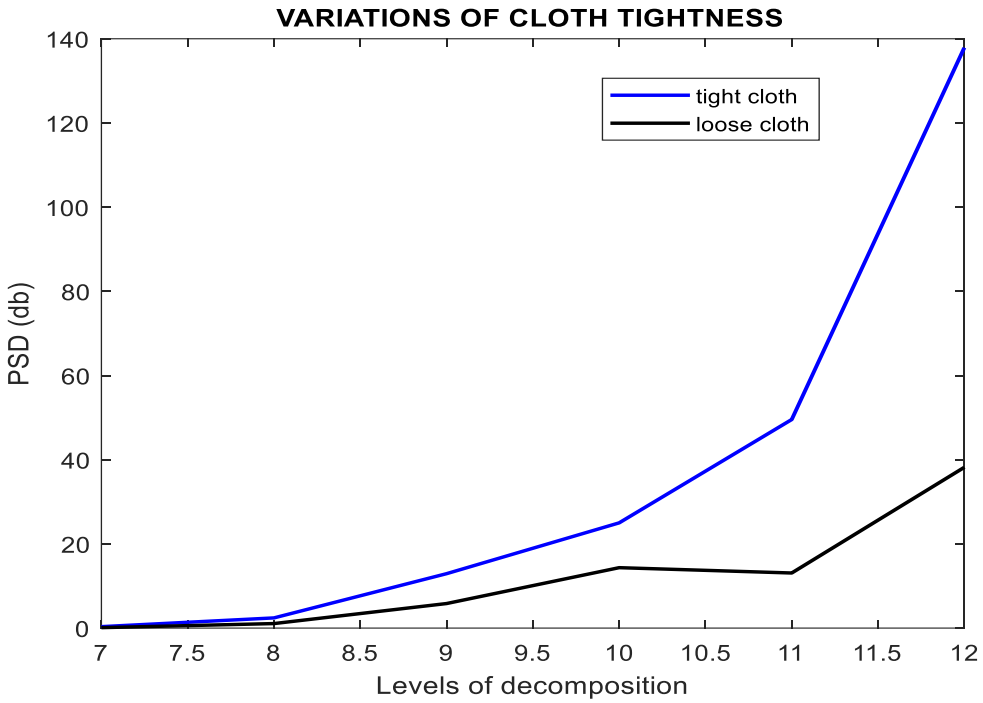

Figure 14: Variability of LDV's power spectral density with cloth tightness

Variability of LDV's power spectral density with skin color

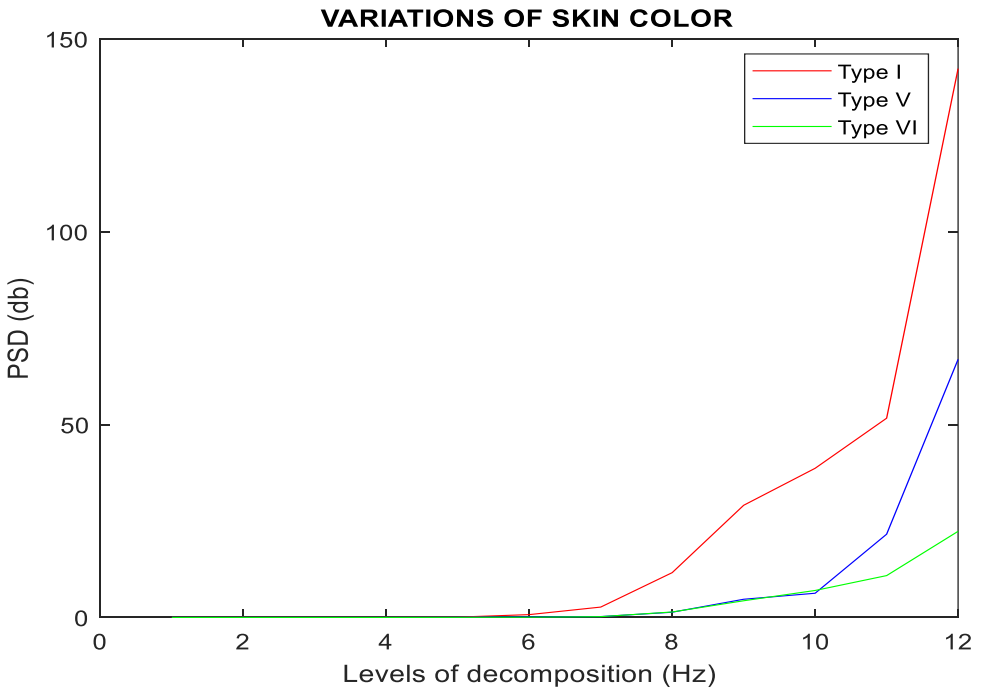

Figure 15: Variability of LDV's power spectral density with skin color

3.3. Validation of the LDV signal with the pulse signal

Table having various parameters considered in the calculation of heart beats and respiratory rates numbers.

Table 3: Features extracted from the filtered signal to calculate heart rate and respiratory rates per minute. PSD_ HR, PSD_RR=Power spectral density of Heart rate and respiratory rate, RMS_HR, RMS_RR=Root Mean Square value for heart rate and respiratory rate, P2P_HR and P2P_RR=Peak to Peak interval for heart rate and respiratory rate, Disp._HR and Disp._HR=displacement of the chest due to heart rate and respiratory rate.

Variable	*Values*	*PSD_HR*	*PSD_RR*	*RMS_HR*	*RMS_HR*	*P2P_HR*	*P2P_RR*	*Disp._HR*	*Disp._HR*	*H.Beat*	*R.Rate*
Distance (m)	***0.5***	*0.00898*	*0.00178*	*0.17075*	*0.08152*	*0.75240*	*4.0143*	*0.00399*	*0.02583*	*75±12*	*19±4*
	1	*0.00878*	*0.00157*	*0.17076*	*0.08192*	*0.75241*	*4.11431*	*0.00387*	*0.02573*	*79±15*	*18±3*
	2	*0.00887*	*0.00167*	*0.17147*	*0.08201*	*0.75239*	*4.11092*	*0.00394*	*0.02573*	*79±16*	*18±4*
	3	*0.00887*	*0.00166*	*0.17146*	*0.08202*	*0.75233*	*4.09536*	*0.00396*	*0.02572*	*79±14*	***17**±5*
	5	*0.00740*	*0.00156*	*0.15462*	*0.07372*	*0.74592*	*3.93004*	*0.00263*	*0.02124*	*80±18*	*15±8*
Angles (degrees)											
	0	*0.00582*	*0.00087*	*0.13728*	*0.05584*	*0.74680*	*3.96846*	*0.00199*	*0.01770*	*80±15*	*20±6*
	10	*0.00753*	*0.00162*	*0.15607*	*0.07515*	*0.74806*	*3.95734*	*0.00269*	*0.02224*	*80±16*	*19±5*
	20	*0.00753*	*0.00163*	*0.15603*	*0.07530*	*0.74783*	*3.95479*	*0.00266*	*0.02234*	*80±18*	*18±4*
	30	*0.01228*	*0.00497*	*0.19669*	*0.12859*	*0.74742*	*4.38541*	*0.00229*	*0.03307*	*80±17*	*18±4*
	40	*0.00751*	*0.00163*	*0.15583*	*0.07537*	*0.74759*	*3.95237*	*0.00265*	*0.02229*	*80±18*	*18±5*
	45	*0.00753*	*0.00164*	*0.15600*	*0.07555*	*0.74747*	*3.94863*	*0.00265*	*0.02228*	*80±17*	*18±4*
	60	*0.01280*	*0.00513*	*0.20049*	*0.13096*	*0.74800*	*4.38623*	*0.00240*	*0.03372*	*80±15*	*19±6*
	70	*0.01279*	*0.00523*	*0.20049*	*0.13240*	*0.74763*	*4.39315*	*0.00236*	*0.03487*	*80±14*	*19±5*
	80	*0.0112*	*0.02223*	*0.18821*	*0.25536*	*0.74988*	*4.47538*	*0.00351*	*0.06655*	*80±18*	*18±6*

Plots of heart rate distribution with distance and angles

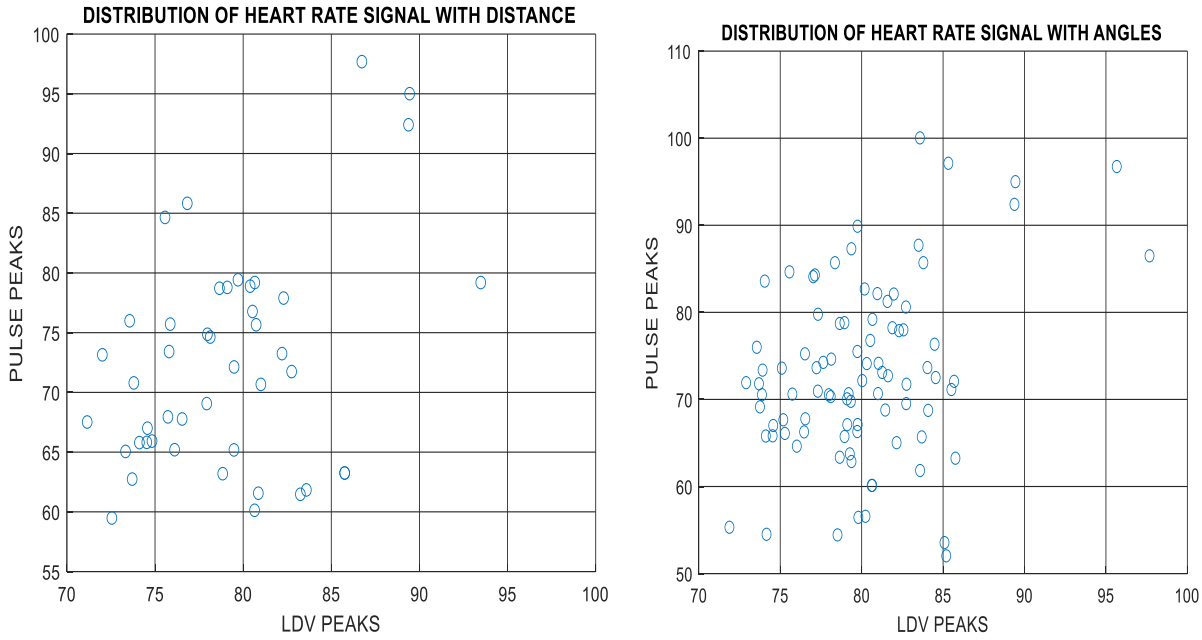

Figure 16: Distribution of heart beats by LDV plotted against the heart beats from Finger pulse reader

Distribution of respiratory peak to peak intervals of signals obtained using LDV device with a standard breathing protocol of 4 seconds

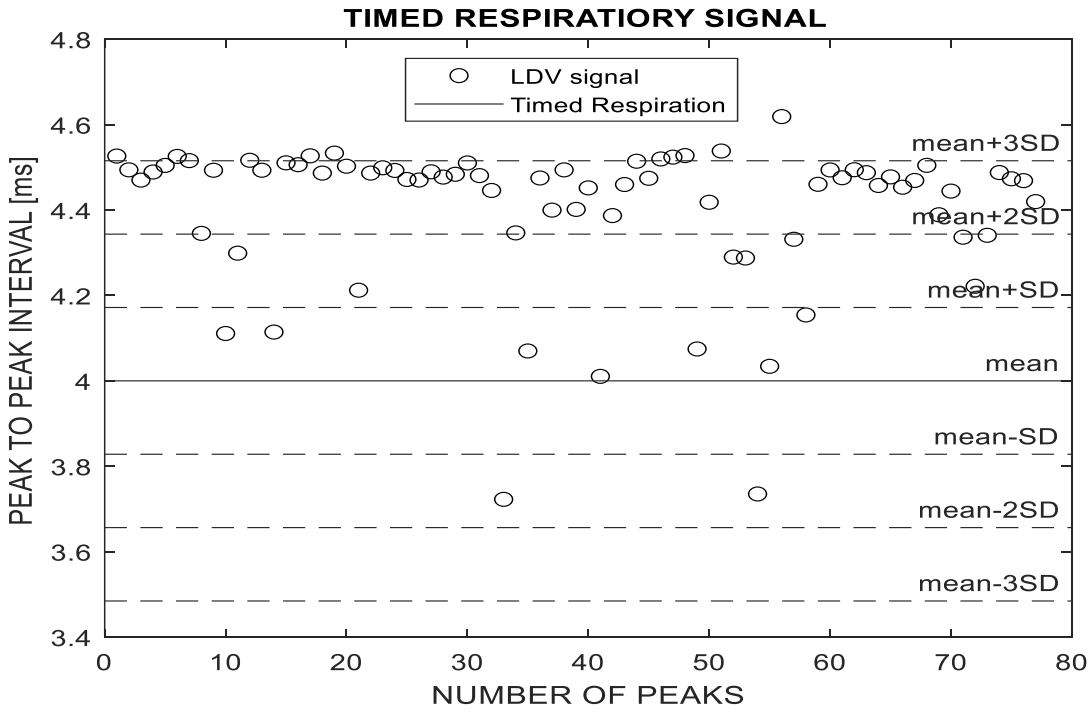

3.4. Result of the developed models

Accuracy of the trained models

Table 4: The accuracy and precision of the **1st model** trained with the data collected only from the chest anatomical positions of subjects using the decision tree classification algorithm

	precision	*recall*	*f1-score*	*support*
0.0	0.92	0.86	0.89	58518
1.0	0.87	0.93	0.90	58512
accuracy			0.89	117030
macro avg	0.90	0.89	0.89	117030
weighted avg	0.90	0.89	0.89	117030

Table 5: The accuracy and precision of the **2nd model** trained with the data collected from all the subjects using the decision tree classification algorithm

	precision	*recall*	*f1-score*	*support*
0.0	0.92	0.90	0.91	151576
1.0	0.90	0.92	0.91	152572
accuracy			0.91	304148
macro avg	0.91	0.91	0.91	304148
weighted avg	0.91	0.91	0.91	304148

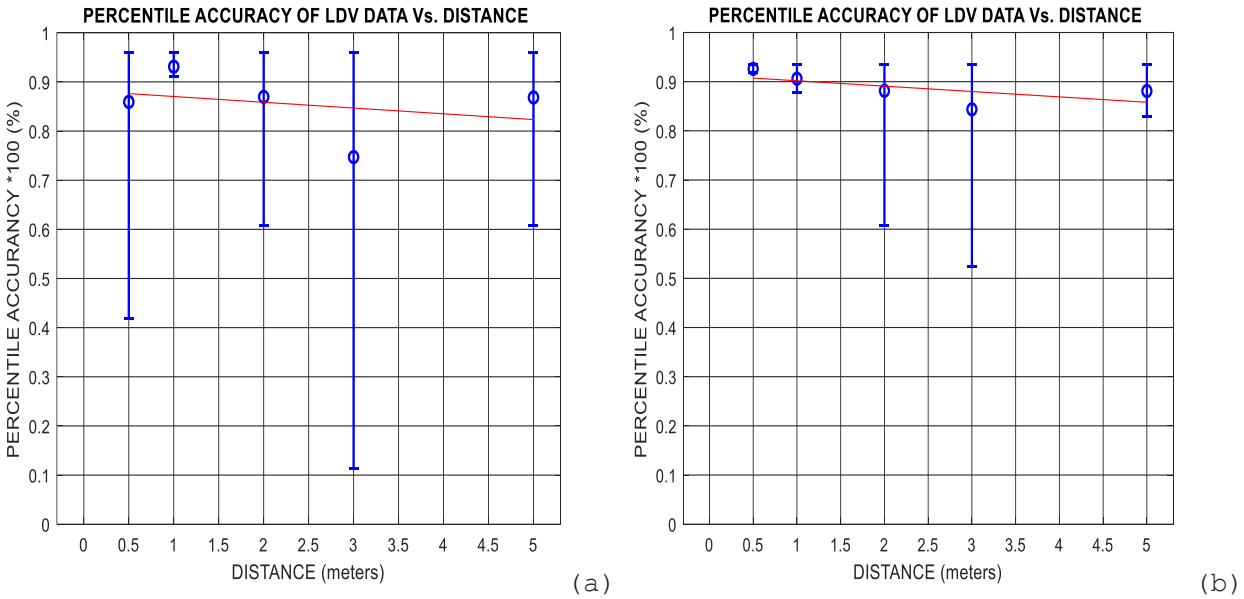

Figure 17: The mean percentile (50%), high percentage (90%) and low percentile (10%) accuracies of the classified human subject data varying with distance. (a). Error plot of data classified using the 1st model. (b) Error plot of data classified using the 2nd model

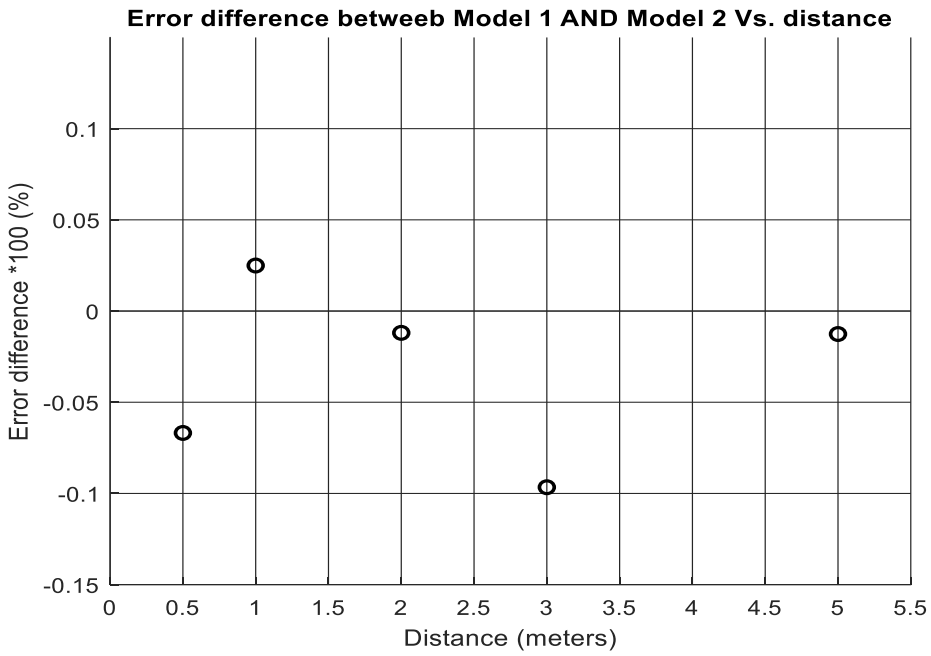

Figure 18: Error difference between the accuracy of model 1 and model 2 with distance

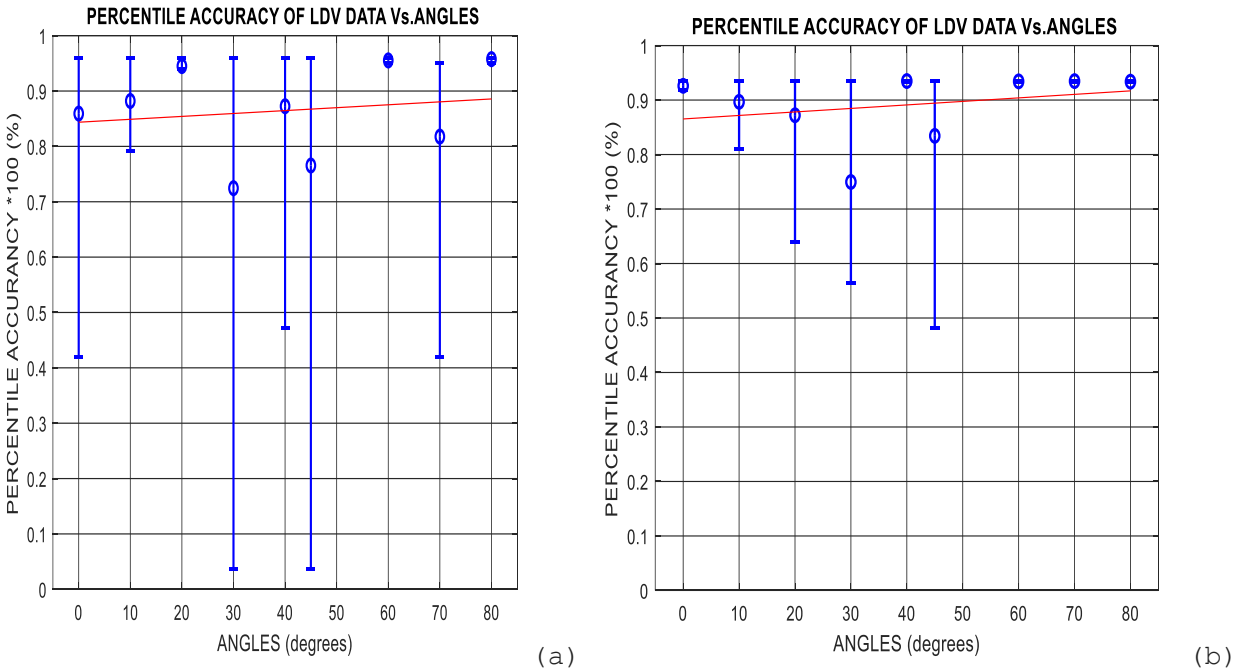

Figure 19: The mean percentile (50%), high percentage (90%) and low percentile (10%) accuracies of the classified human subject data varying angles. (a). Error plot of data classified using the 1st model. (b) Error plot of data classified using the 2nd model.

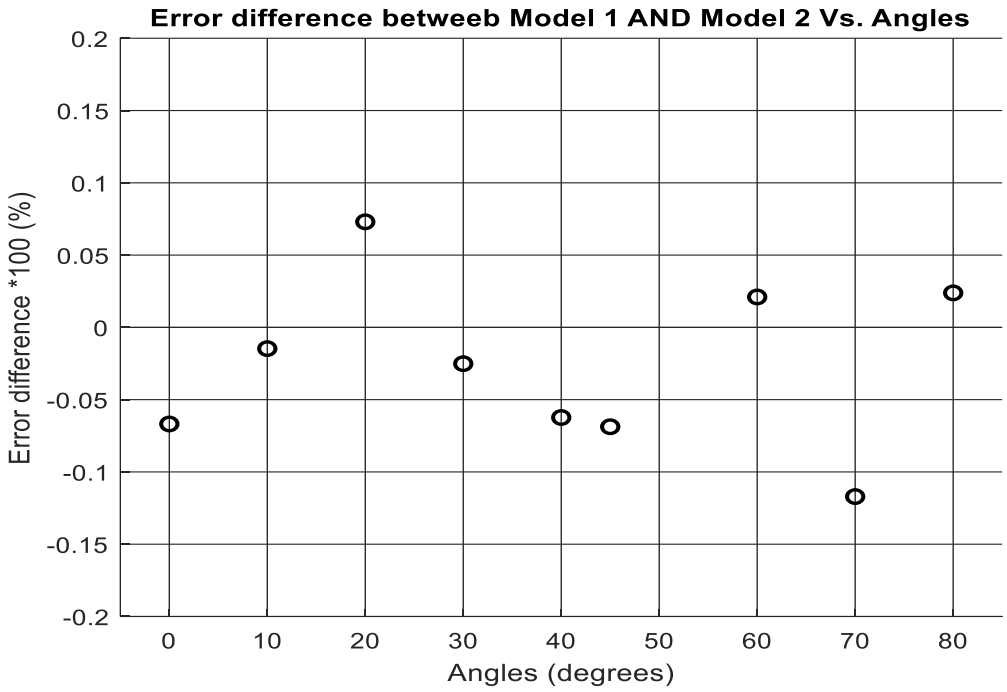

Figure 20: Error difference between the accuracy of model 1 and model 2 with Angles

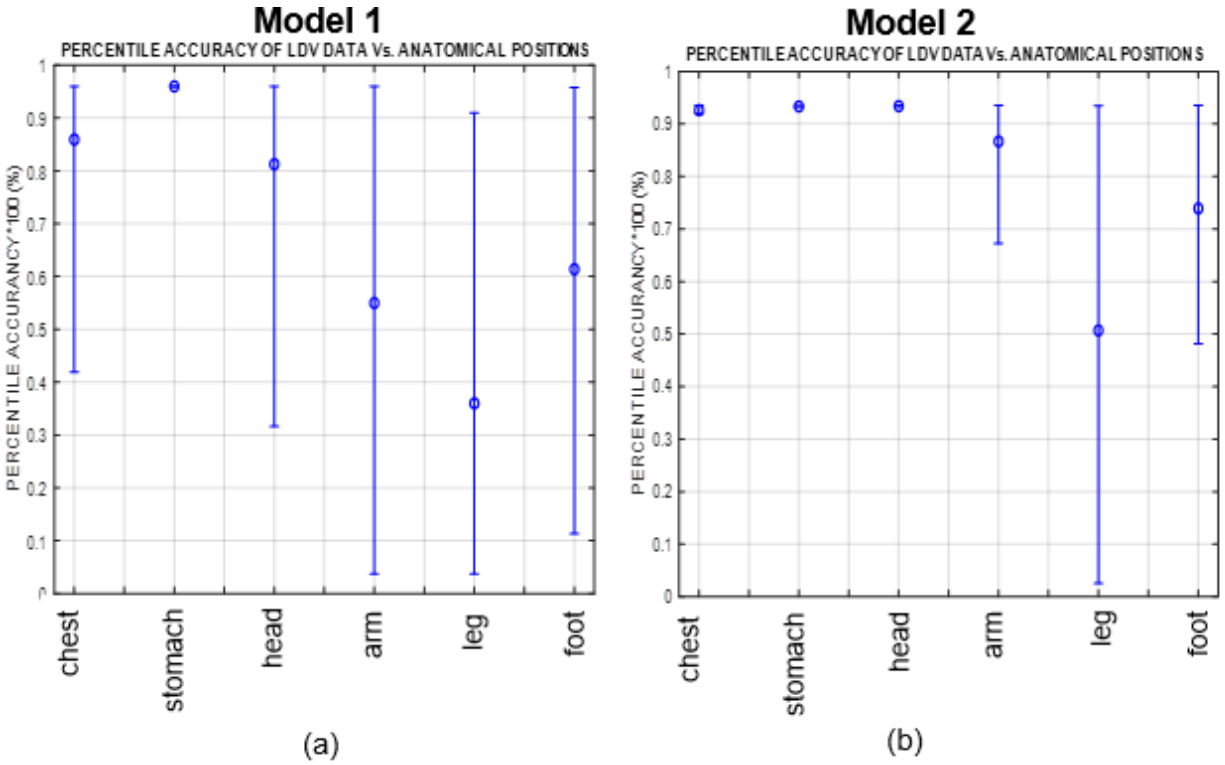

Figure 21The mean percentile (50%), high percentage (90%) and low percentile (10%) accuracies of the classified human subject data varying with anatomical positions. (a). Error plot of data classified using the 1st model. (b) Error plot of data classified using the 2nd model.

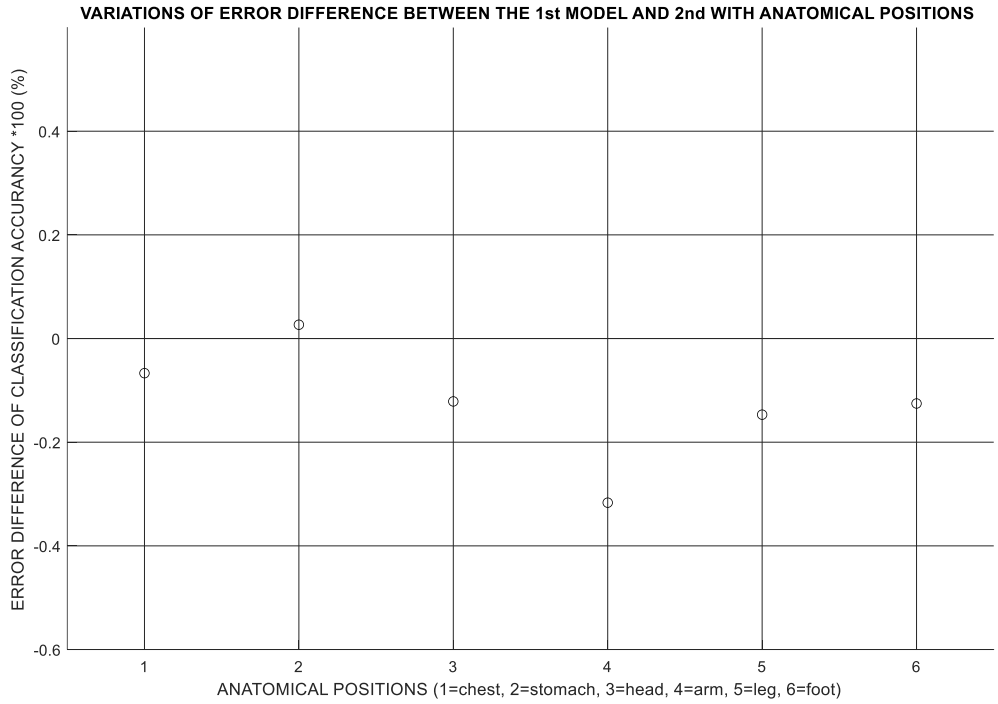

Figure 22: Error difference between the accuracy of model 1 and model 2 with Anatomical positions

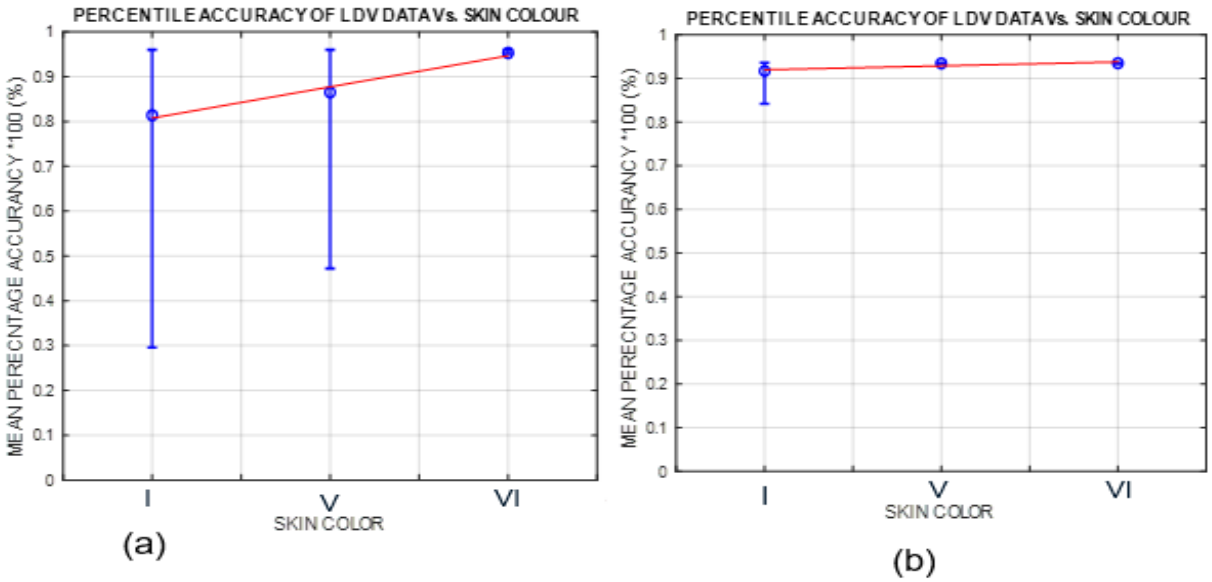

Figure 23: The mean percentile (50%), high percentage (90%) and low percentile (10%) of the classified subject data varying with skin color. (a). Data classified using the 1st model. (b) Data classified using the 2nd model.

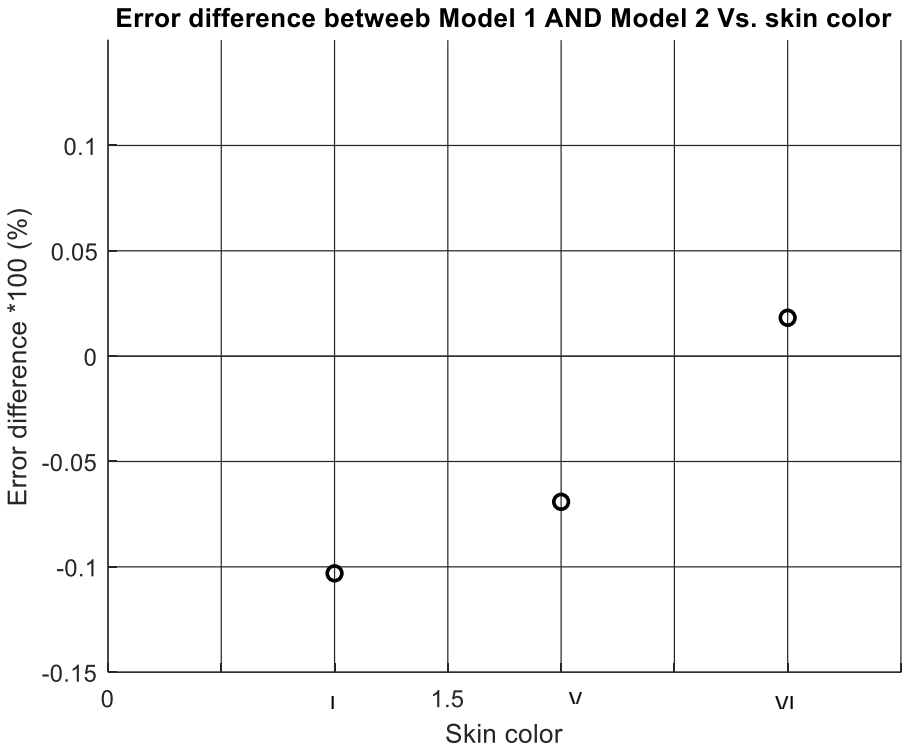

Figure 24: Error difference between the accuracy of model 1 and model 2 with skin color

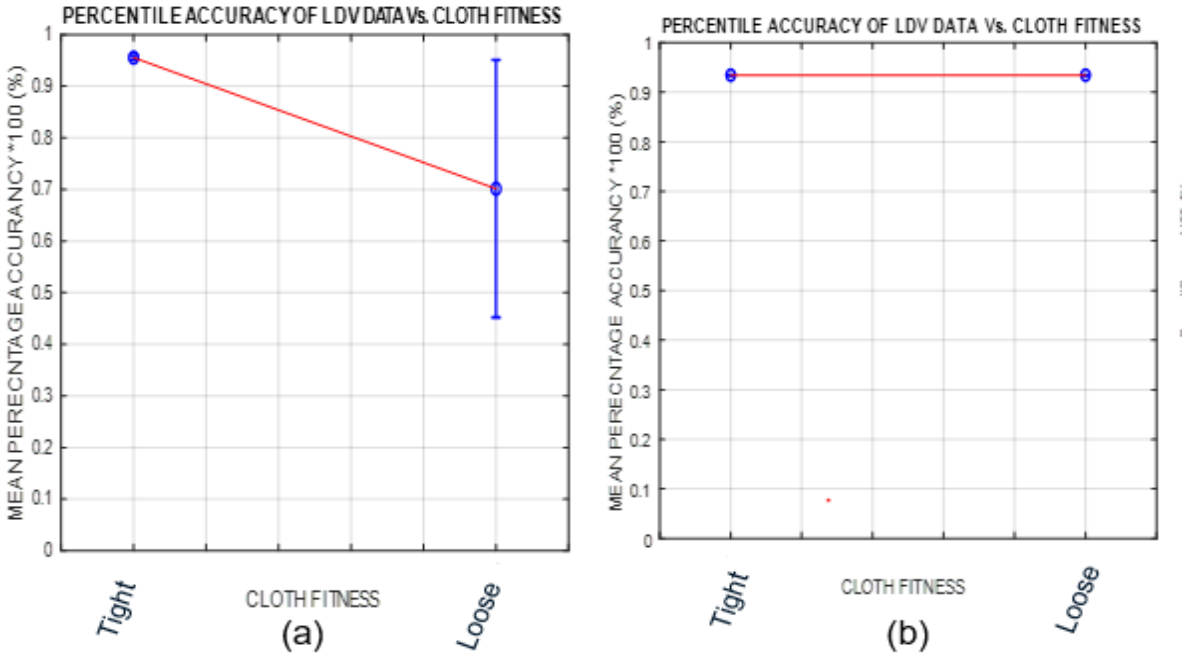

Figure 25: The mean percentile (50%), high percentage (90%) and low percentile (10%) of the classified subject data varying with skin color. (a). Data classified using the 1st model. (b) Data classified using the 2nd model.

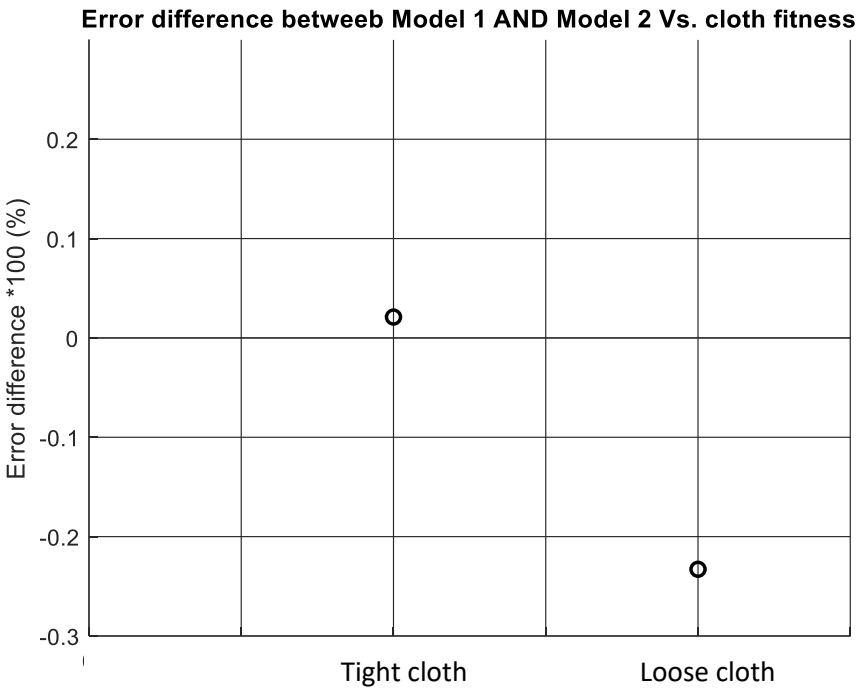

Figure 26: Error difference between the accuracy of model 1 and model 2 with cloth fitness

CHAPTER 4

4. DISCUSSIONS

The main objective of this study was to develop a model that considers the various parameters affecting the LDV signals during acquisition like distances of the subject from the device, angle at which the device's laser beam is directed to the subject, the effect of different anatomical positions, the behavior of the signal with different skin color and as well as the influence of a cloth's tightness on the signal. The study builds on the success of previous studies by Scalise et al. [28-30], Morbiducci et al. [25] and, Marchionni et al. [31] that have been able to demonstrate the ability of laser doppler vibrometry technique to detect heart rate and respiratory rate vital sign signals from both a baby and an adult.

17 adults between the age of 21 and 30 years were recruited for this study. From each subject, more that 9 data points were collected i.e., data while varying the distances, angles, anatomical positions, and cloth tightness. Using wavelet decomposition with 7 decibel (db) and levels 12, the distribution of energies was well understood (Figure 6). The red colored levels are for respiratory signals with frequencies of (0.1 to 0.5 Hz) and the green ones are for heart rate signals with frequencies of (0.5 to 5 Hz). In Figure 7 and 10, the LDV's acquired signal was compared with the pulse reader signal and similarities in the numbers of respiratory cycle numbers and the position of heart rate peaks could easily been seen. Upon filtering for respiratory signal at a frequency between (0.1 to 0.5 Hz) as shown in Figure 8, the signal had the highest amplitude from the stomach because of the diaphragm contractions, followed by chest due to the movement of the rib cages during breathing, then the signal from the arm, head, leg, and foot followed subsequently due to the pulsatile behavior of blood flow affected by respiratory activity. Figure 9 shows the heat rate variability from different anatomical positions after being filtered from the raw signals at frequencies between (1-5Hz). The chest had the highest amplitude due to the position of the heart, this is followed by the head due to the numerous numbers of vessels supplying it with blood, followed with the stomach, then arm, leg and foot that have blood vessels delivering blood at low velocities with little displacement activities.

Signals subjected to different LDV parameter variables were then analyzed to understand their variabilities. In Figure 11, the variability of distances with the power density were plotted and with distance 0.5meters registering higher power compared to other distances. This is because there are so many agents and particles in the environments that reduce the strength of the signal as distance is increased through absorption, reflection, and scattering. In Figure 12, the variability of the angle of acceptance were analyzed and it was shown to have a stability until 60 degrees then the power starts dropping. Figure 13 shows power density distribution in different anatomical positions with the stomach having the highest and least in the foot. A subject putting on a loose cloth registers a low power LDV signal as compared to one putting on a tight cloth (Figure 14). This is because the tight cloth is equally displaced with the same intensities and speed compared to a loose cloth when the heart contracts or diaphragm and rib cages move due to respiration. Finally, the LDV signals have a high absorptive tendency when the beam is pointed to skin with a color scale of VI compared to V or I. As a result, a subject with a color scale of VI has a lower power compared to the ones having a V or I (Figure 15).

In the table 3, different features were extracted from the signal such as power spectral density used earlier in the analysis, root mean square vales, peak to peak intervals used to calculate heart rates and respiratory rates and displacements because of heart activities or respiratory activities. The range of displacements caused by heart activities was between 0.0015mm to 0.004 mm and that due to respiratory activities were between 0.016 to 0.067mm. With this table, the number of beats from the heart and respiratory cycles per minute were determined and plotted with pulse reader values. As shown in Figure 16, the distribution of heart rates due to the finger pulse reader were between 59 to 98 beats per minute and the one of LDV was 70 to 93 beats per minute. Figure 17 illustrated the distributions of peak-to-peak intervals of the LDV signals with a standard breathing protocol of 4second and the range were between 3.7s to 4.6s.

After studying the effects of various parameters on the LDV signals, the data set from the subjects were then trained with data from a baby mannequin and other random objects from the environment to imitate the harsh environments. The 1st model was trained with 70% of the data obtained from the chest of the subject at 0.5m and an angle of 0 degrees had an accuracy of 0.89 as shown in Table 4 and the 2nd model that was trained with 70% of all the data set acquired from

the different protocols performed better with an accuracy of 0.91. An error plot of the data accuracies trained with the 1st and 2nd model were plotted against distance (Figure 17 (a) and (b)) and a descending trend of the mean was observed as the distance was being increased. This corresponds to the effect of signal loss due to the numbers of factors like refraction, reflection, interference, and absorption by environmental objects. The difference in the accuracies between the two models suggests that the 2nd model had a better classification performance compared to the 1st model (Figure 18, 20, 22, 24, and 25) due to the large data sets it registered during the training. The error plot of the two models with angles had more stable and gradual increasing trend (Figure 19 (a) and (b)) as stated by the LDV manufacturer. This is contrary to the error plots of the two models with anatomical positions, skin color and cloth fitness that all had an increasing mean percentile trend (Figure 21, 22,23 (a) and (b)) due to discontinuity in their variability. The low percentile values in all the plots had a greater deviation from the mean percentile. The mean accuracy of the first model used in classifying the different anatomical positions is 65.8% and its standard deviation is 22.4%. For the second model, its mean accuracy is 80.0% with a standard deviation of 16.9%.

CHAPTER 5

5. CONCLUSIONS

Contactless measurements of cardiorespiratory vital is very crucial for application in hard-to-reach environment. This is because it allows signal acquisition of a trapped person without endangering their life and the life of the attendants or medical personal. Laser Doppler vibrometry technique is in the category of these contactless methods. Both model 1 and model 2 can uniquely classify human subjects from other objects within the environment with the mean accuracies of 0.829and 0.92, respectively. The performance of the second model on all the data collected from the human subjects had a better classification accuracy with scores above 0.72 across all the various parameters like distances, angles, anatomical positions, skin color and cloth fitness signals except for signals from the leg that had a classification accuracy score of 0.5.

Using our second developed model, the detection of state of life for an individual trapped in a hard-to-reach environment can easily be determined with an accuracy above 0.9, giving us less errors compared to the first model. After that, the data can be subjected to a MATLAB algorithm to detect the number of peaks and peak to peak intervals for both respiration and heart rate. The intervals between each peak are then used to calculate the number of heart beats and respiratory cycles from each signal

5.1. Future works

We plan to develop another model using purely statical methods and then compare their results with the currently developed model. All the models will then be deployed in the field for evaluation while simulating hard to reach environments. The model that will outperform the other will then be incorporated into the hardware to develop a deployable equipment to save the lives of those trapped.

CHAPTER 6

REFERENCES

1. Max Roser, Joe Hasell, Bastian Herre and Bobbie Macdonald (2016) - "War and Peace". *Published online at OurWorldInData.org.* Retrieved from: 'https://ourworldindata.org/war-and-peace' [Online Resource]
2. Mamady Kebe, Rida Gadhafi, Baker Mohammad, Mihai Sanduleanu, Hani Saleh and Mahmoud Al-Qutayri. Human Vital Signs Detection Methods and Potential Using Radars: A Review. Sensors 2020, 20, 1454; doi:10.3390/s20051454
3. Barrett, K.E.; Barman, S.M.; Brooks, H.L.; Yuan, J.X.-J.; Ganong, W.F. Ganongs Review of Medical Physiology; McGraw-Hill Education: New York, NY, USA, 2019
4. What Should My Heart Rate Be? Available online: https://www.medicalnewstoday.com/articles/235710.php (accessed on 26 January 2020).
5. Atlef, J.L. Principles of Clinical Electrocardiography. Anesthesiology 1980, 52, 195. [CrossRef]
6. Dutta, D.N.; Das, R.; Pal, S. Automated Real-Time Processing of Single Lead Electrocardiogram for Simultaneous Heart Rate and Respiratory Rate Monitoring. J. Med. Devices 2017, 11. [CrossRef]
7. Schmidt, M.; Schumann, A.; Müller, J.; Bär, K.-J.; Rose, G. ECG derived respiration: Comparison of time-domain approaches and application to altered breathing patterns of patients with schizophrenia. Physiol. Meas. 2017, 38, 601–615. [CrossRef]
8. Hallfors, N.; Jaoude, M.A.; Liao, K.; Ismail, M.; Isakovic, A. Graphene oxide—Nylon ECG sensors for wearable IoT healthcare. In Proceedings of the 2017 Sensors Networks Smart and Emerging Technologies (SENSET), Beirut, Lebanon, 12–14 September 2017
9. Stingeni, L.; Cerulli, E.; Spalletti, A.; Mazzoli, A.; Rigano, L.; Bianchi, L.; Hansel, K. The role of acrylic acid impurity as a sensitizing component in electrocardiogram electrodes. Contact Dermat. 2015, 73, 44–48. [CrossRef]
10. Allen, J. Photoplethysmography and its application in clinical physiological measurement. Physiol. Meas. 2007, 28, R1. [CrossRef] [PubMed]
11. Massaroni, C.; Nicolò, A.; Presti, D.L.; Sacchetti, M.; Silvestri, S.; Schena, E. Contact-Based Methods for Measuring Respiratory Rate. Sensors 2019, 19, 908. [CrossRef] [PubMed]
12. Shao, D.; Liu, C.; Tsow, F.; Yang, Y.; Du, Z.; Iriya, R.; Yu, H.; Tao, N. Noncontact Monitoring of Blood Oxygen Saturation Using Camera and Dual-Wavelength Imaging System. IEEE Trans. Biomed. Eng. 2016, 63, 1091–1098. [CrossRef]
13. Meredith, D.J.; Clifton, D.; Charlton, P.; Brooks, J.; Pugh, C.W.; Tarassenko, L. Photoplethysmographic derivation of respiratory rate: A review of relevant physiology. J. Med. Eng. Technol. 2011, 36, 1–7. [CrossRef]
14. Moll, J.M.; Wright, V. An objective clinical study of chest expansion. Ann. Rheum. Dis. 1972, 31, 1–8. [CrossRef] [PubMed]
15. Sinha, R. An Approach for Classifying ECG Arrhythmia Based on Features Extracted from EMD and Wavelet Packet Domains. Master Dissertation. 2012. Available online: https://www.researchgate.net/publication/287200946_An_Approach_for_Classifying_ECG_Arrhythmia_ Based_on_Features_Extracted_from_EMD_and_Wavelet_Packet_Domains. (accessed on 3 March 2020).

16. Berntson, G.G.; Cacioppo, J.T.; Quigley, K.S. Respiratory sinus arrhythmia: Autonomic origins, physiological mechanisms, and psychophysiological implications. Psychophysiology 1993, 30, 183–196. [CrossRef] [PubMed]
17. Massaroni, C.; Nicolò, A.; Presti, D.L.; Sacchetti, M.; Silvestri, S.; Schena, E. Contact-Based Methods for Measuring Respiratory Rate. Sensors 2019, 19, 908. [CrossRef] [PubMed]
18. S. Y. Chekmenev, H. Rara, and A. A. Farag, ‘‘Non-contact, wavelet-based measurement of vital signs using thermal imaging,’’ in Proc. 1st Int. Conf. Graph., Vis., Image Process., Cairo, Egypt, 2005, pp. 107–112.
19. Q.-L. Yan, Z.-W. Song, X.-B. Shi, Z.-Y. Yang, and X.-H. Zhang, ‘‘Combustion mechanism of double-base propellant containing nitrogen heterocyclic nitroamines (II): The temperature distribution of the flame and its chemical structure,’’ Acta Astron., vol. 64, no. 5, pp. 602–614, 2009
20. J. Allen, ‘‘Photoplethysmography and its application in clinical physiological measurement,’’ Physiol. Meas., vol. 28, no. 3, pp. R1–R39, 2007
21. K. Nakajima, Y. Matsumoto, and T. Tamura, ‘‘Development of real-time image sequence analysis for evaluating posture change and respiratory rate of a subject in bed,’’ Physiol. Meas., vol. 22, pp. 21–28, Aug. 2001
22. Wang, G.; Munoz-Ferreras, J.-M.; Gu, C.; Li, C.; Gomez-Garcia, R. Application of Linear-Frequency-Modulated Continuous-Wave (LFMCW) Radars for Tracking of Vital Signs. IEEE Trans. Microw. Theory Tech. **2014**, 62,1387–1399. [CrossRef]
23. Wisland, D.T.; Granhaug, K.; Pleym, J.R.; Andersen, N.; Stoa, S.; Hjortland, H.A. Remote monitoring of vital signs using a CMOS UWB radar transceiver. In Proceedings of the 2016 14th IEEE International New Circuits and Systems Conference (NEWCAS), Van Couver, BC, USA, 26–29 June 2016; pp. 1–4.
24. C. P. Wang, ‘‘Laser doppler velocimetry,’’ J. Quant. Spectrosc. Radiat. Transf., vol. 40, no. 3, pp. 309–319, 1988
25. U. Morbiducci, L. Scalise, M. De Melis, and M. Grigioni, ‘‘Optical vibrocardiography: A novel tool for the optical monitoring of cardiac activity,’’ Ann. Biomed. Eng., vol. 35, no. 1, pp. 45–58, Jan. 2007.
26. Paone, N., Scalise, L. & Tomasini, E. P. (2009) Laser doppler velocimetry. In: G. C. Righini, A. Tajani, A. Cutolo (Eds.), An introduction to optoelectronic sensors, Hackensack, NJ: World Scientific
27. Habib Tabatabai, David E. Oliver, John W. Rohrbaugh, and Christopher Papadopoulos. Novel Applications of Laser Doppler Vibration Measurements to Medical Imaging. Sens Imaging (2013) 14:13–28
28. L. Scalise and U. Morbiducci, ‘‘Non-contact cardiac monitoring from carotid artery using optical vibrocardiography,’’ Med. Eng. Phys., vol. 30, no. 4, pp. 490–497, 2008
29. L. Scalise, P. Marchionni, and I. Ercoli, ‘‘Optical method for measurement of respiration rate,’’ in Proc. IEEE Int. Workshop Med. Meas. Appl., May 2010, pp. 19–22
30. L. Scalise, I. Ercoli, P. Marchionni, and E. P. Tomasini, ‘‘Measurement of respiration rate in preterm infants by laser Doppler vibrometry,’’ in Proc. IEEE Int. Workshop Med. Meas. Appl., May 2011, pp. 657–661.
31. P. Marchionni, L. Scalise, I. Ercoli, and E. Tomasini, ‘‘An optical measurement method for the simultaneous assessment of respiration and heart rates in preterm infants,’’ Rev. Sci. Instrum., vol. 84, no. 12, p. 121705, 2013
32. Antonino Caizzone, Assim Boukhayma, Christian Enz. A 2.6 uW Monolithic CMOS Photoplethysmographic (PPG) Sensor Operating with 2 µW LED Power for Continuous

Health Monitoring. DOI 10.1109/TBCAS.2019.2944393, IEEE Transactions on Biomedical Circuits and Systems.
33. Craig A. Manifold, Neil Davids, Lance C. Villers, and David A. Wampler. Capnography for the Nonintubated Patient in the Emergency setting. The Journal of Emergency Medicine, Vol. 45, No. 4, pp. 626–632, 2013
34. Guanghao Sun, Yosuke Nakayama, Sumiyakhand Dagdanpurev, Shigeto Abe, Hidekazu Nishimura, Tetsuo Kirimoto, Takemi Matsui. Remote sensing of multiple vital signs using a CMOS camera-equipped infrared thermography system and its clinical application in rapidly screening patients with suspected infectious diseases. G. Sun et al. / International Journal of Infectious Diseases 55 (2017) 113–117

APPENDIX

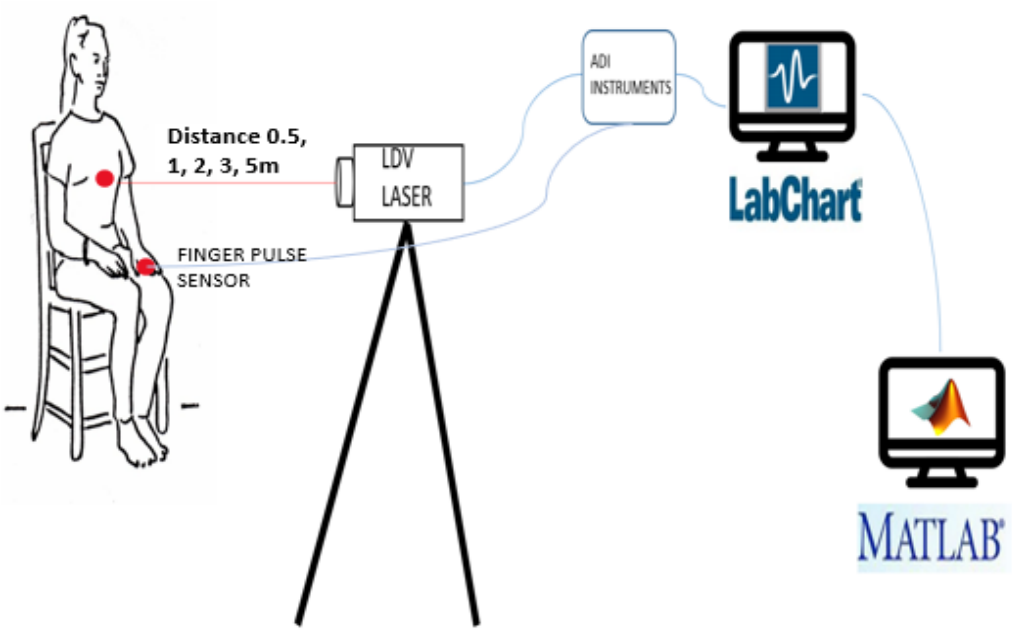

Figure 27: Experimental setup for signal acquisition from the chest anatomical position while varying distances.

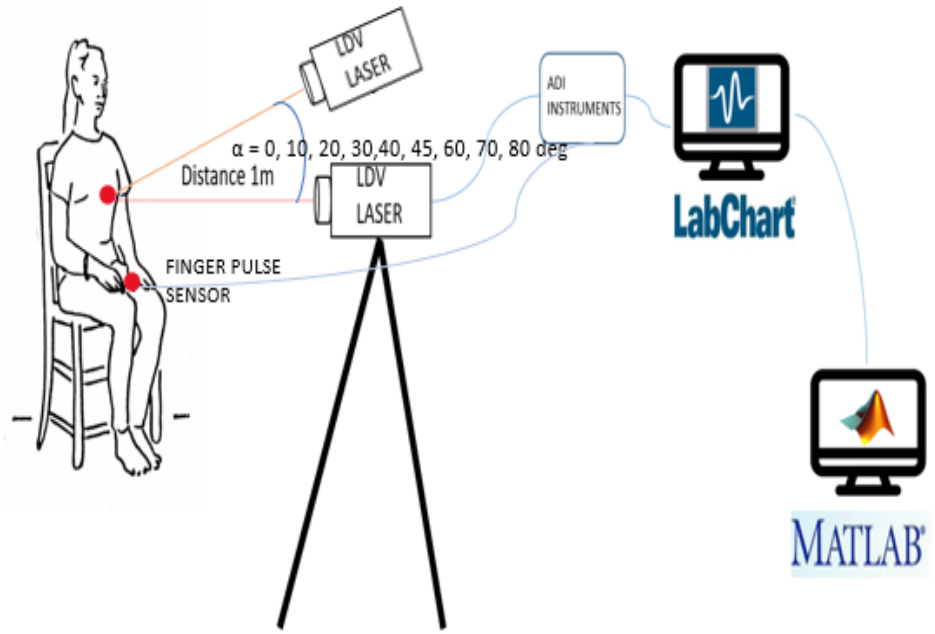

Figure 28: Experimental setup for signal acquisition from the chest anatomical position while varying angles of acceptance.

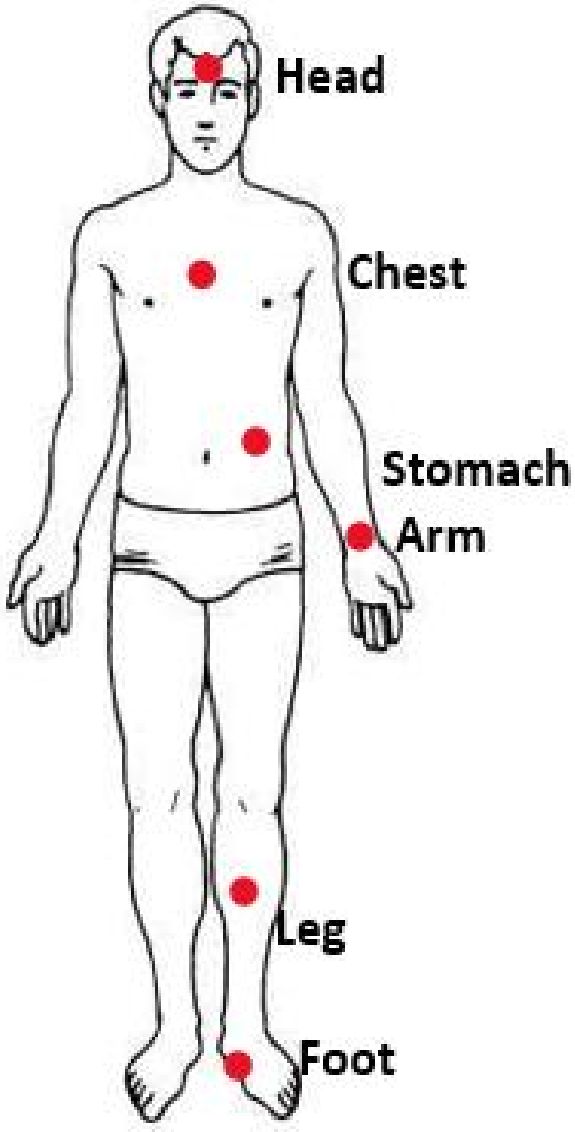

Figure 29: Anatomical Positions that were evaluated with LDV device for cardiorespiratory vital signs signal presence

PDV-100 General	
Velocity ranges	3: (± 20 mm/s, ± 100 mm/s, ± 500 mm/s)
Frequency range	0 to 22 kHz
Scaling factor	5 mm/s/V, 25mm/s/V, 125 mm/s/V
Velocity resolution	≤ 0.05 µm/s (in 1 Hz resolution bandwidth)
Working distance	0.2 m to > 30 m
Laser safety	Eye safe, class II visible HeNe laser

PDV-100 Output signals	
Analog velocity	± 4 Volts full scale, 24 bits resolution, BNC connector Frequency range < 0.5 Hz to 22 kHz
Digital velocity	S/P-DIF standard, 24 bits resolution, 48 kSa/s Frequency range 0 Hz to 22 kHz
Digital low pass filter	1 KHz, 5 kHz, 22 kHz (-0.1 dB), roll-off 120 dB /decade
Analog high pass filter	100 Hz (-3 dB), roll-off 60 dB /decade
Calibration accuracy	Analog output: 1% (20 Hz – 22 kHz) Digital output: 0.1% (0.05 Hz – 22 kHz)

PDV-100 Housing and Power	
Dimensions	66 x 129 x 290 mm
Weight	2.6 kg
Protection Rating	IP-64 Standard dust and water-resistant housing
Temperature range	0° to 40 ° C (to 45° C for intermittent operation up to 30 min.)
Display	Illuminated 3 line LCD
Power	11 ... 14,5 V DC, maximum 15 W
Batteries	2 rechargeable Li-Ion batteries for nominal 5 hours operation time

PDV-100 Accessories	
Included	AC mains adapter, manual, calibration certificate 1 page of reflective tape S/P-DIF interface cable (Triax to RCA)
Optional	■ Transportation bag with 2 LiOH batteries and charger ■ Cigarette lighter socket adapter & cable ■ Compact tripod ■ Additional battery set

Figure 30: An image of the LDV device of type PDV-100 and its outline specifications

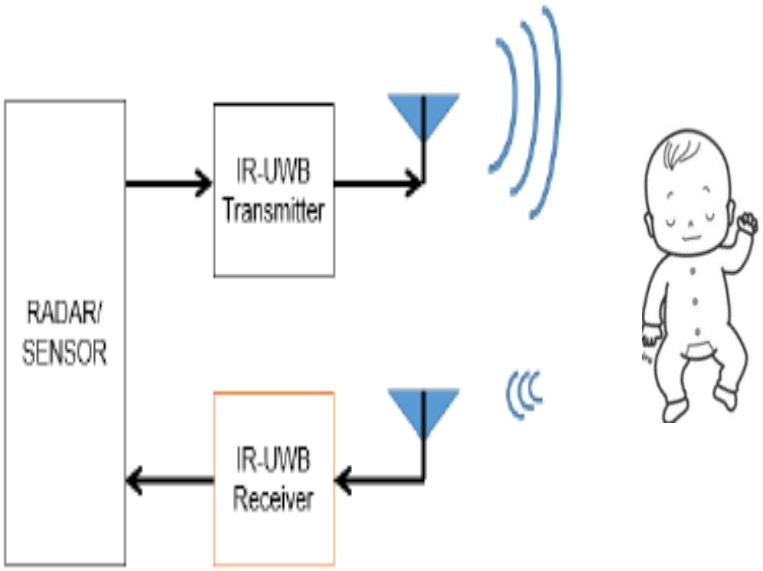

Figure 31: Ultra-Wide Band (UWB) radar systems

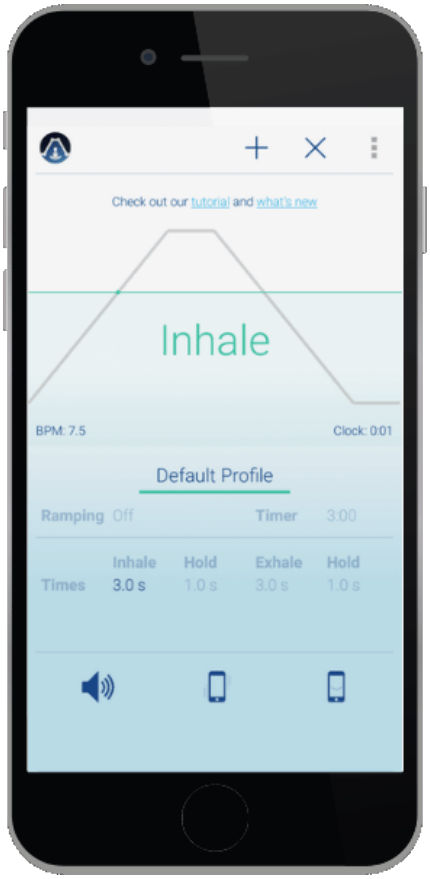

Figure 32: Standard breathing Application. Image from https://www.othership.us/resources/4-7-8-breathing-apps

Python Training Code

```
# Load libraries
import numpy as np # linear algebra
import pandas as pd # data processing, CSV file I/O (e.g. pd.read_csv)
from sklearn.model_selection import train_test_split
from sklearn.model_selection import cross_validate
from sklearn.model_selection import KFold
from sklearn.tree import DecisionTreeClassifier
from sklearn.ensemble import RandomForestClassifier
from sklearn import metrics

import matplotlib.pyplot as plt
from sklearn.tree import plot_tree

import json
import pandas
from pandas.plotting import scatter_matrix

import matplotlib.pyplot as plt
from sklearn import model_selection
from sklearn.metrics import classification_report
from sklearn.metrics import confusion_matrix
from sklearn.metrics import accuracy_score
from sklearn.metrics import roc_curve
from sklearn.metrics import auc
from sklearn.ensemble import RandomForestClassifier
from sklearn.neighbors import KNeighborsClassifier
from sklearn import tree
from sklearn import svm
import pickle
import matplotlib.pyplot as plt
import numpy as np
from scipy import interp
from sklearn import preprocessing
from sklearn.utils.multiclass import unique_labels
from sklearn import tree

import os
import glob
# os.chdir("/directory")


url = "/content/drive/MyDrive/Colab Notebooks/Concat10.csv"
dataset = pd.read_csv(url)


print(dataset.shape)
array = dataset.values
X=array [:0: -1]
print(X.shape)
Y=array [: -1]
print(Y)
```

```
X_train, X_valid, Y_train, Y_valid = train_test_split(X, Y, test_size=0.3,
 random_state=42)

X_train.shape, X_valid.shape, Y_train.shape, Y_valid.shape

X_train_scaled = preprocessing.StandardScaler().fit(X_train).transform(X_t
rain)
X_validation_scaled = preprocessing.StandardScaler().fit(X_train).transfor
m(X_valid)

plt.plot(X_train_scaled[2,:])
plt.plot(X_train[2,:])

base_model = DecisionTreeClassifier(max_leaf_nodes=4, class_weight='balanc
ed')
W=base_model.fit(X_train_scaled, Y_train)

#Create the figure
plt.figure(figsize=(20,10))

#Create the tree plot
tree.plot_tree(W)
plt.show()

predictions=base_model.predict(X_validation_scaled)
print(accuracy_score(Y_valid, predictions))
print(confusion_matrix(Y_valid, predictions))
print(classification_report(Y_valid, predictions))
predictions2=base_model.predict_proba(X_validation_scaled)
print(predictions2)

plt.plot(X_train_scaled[-2,:])
plt.plot(X_train[-2,:])

filename='/content/drive/MyDrive/Colab Notebooks/model_test7.pkl'
pickle.dump(base_model, open(filename, 'wb'))
dataname='/content/drive/MyDrive/Colab Notebooks/model_test7.npy'
np.save(dataname, X_train)
```

Python Testing Code

```
# Load libraries
import numpy as np # linear algebra
from numpy import genfromtxt
import pandas as pd # data processing, CSV file I/O (e.g. pd.read_csv)
from sklearn.model_selection import train_test_split
from sklearn.model_selection import cross_validate
from sklearn.model_selection import KFold
from sklearn.tree import DecisionTreeClassifier
from sklearn.ensemble import RandomForestClassifier

from sklearn import metrics

import matplotlib.pyplot as plt
from sklearn.tree import plot_tree

import json
import pandas
from pandas.plotting import scatter_matrix

import matplotlib.pyplot as plt
from sklearn import model_selection
from sklearn.metrics import classification_report
from sklearn.metrics import confusion_matrix
from sklearn.metrics import accuracy_score
from sklearn.metrics import roc_curve
from sklearn.metrics import auc
from sklearn.ensemble import RandomForestClassifier
from sklearn.neighbors import KNeighborsClassifier
from sklearn import tree
from sklearn import svm
import pickle
import matplotlib.pyplot as plt
import numpy as np
from scipy import interp
from sklearn import preprocessing
from sklearn.utils.multiclass import unique_labels
from sklearn import tree

import os
import glob
# os.chdir("/directory"
```

```
filename='/content/drive/MyDrive/Colab Notebooks/model_test8.pkl'
base_model = pickle.load(open(filename, 'rb'))
X_train=np.load('/content/drive/MyDrive/Colab Notebooks/model_test8.npy')


directory='/content/drive/MyDrive/Colab Notebooks/outfile5/'
di = glob.glob(directory + "*.csv")
print(di)


for file in di:
  print(file)

for file in di:
  x = genfromtxt(file,delimiter=',')
  print(x)
  X = preprocessing.StandardScaler().fit(X_train).transform(x)
  y=base_model.predict_proba(X)
  tab2=np.column_stack((x,y))
  newname = file.split("/")
  filename='/content/drive/MyDrive/Colab Notebooks/RESULT7/PY_'+newname[-
1]
  np.savetxt(filename, tab2, delimiter=",")
print(filename)
```

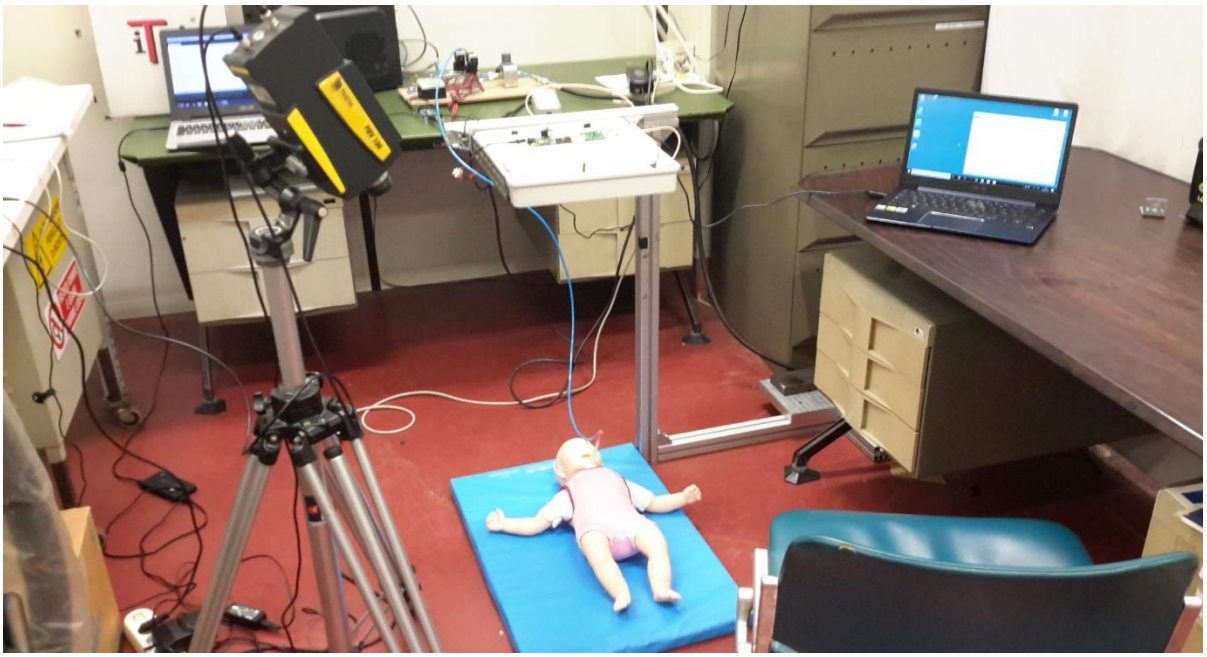

Figure 33: Set up of the LDV while acquiring signal from the baby Mannequin

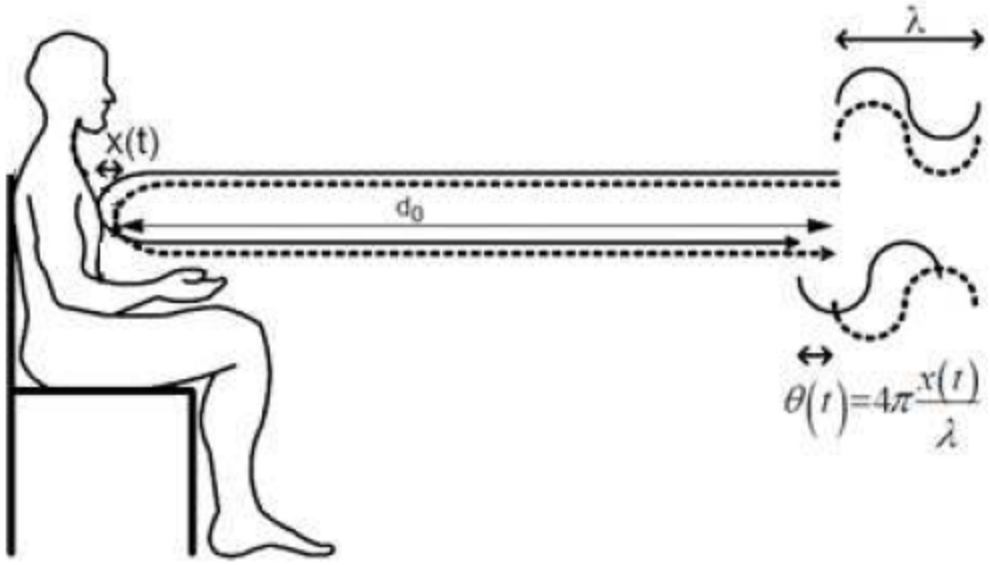

Figure 34: Principle of CW radar monitoring of the chest movement: phase shift Θ(t) caused on the reflected wave by the chest displacement x(t).